Origin, structural geometry, and development of a giant coherent slide: The South Makassar Strait mass transport complex

Cipi Armandita[1,2,3,*], Chris K. Morley[3,4], and Philip Rowell[2,†]

[1]*SKK Migas, Gedung Wisma Mulia Building, Lantai 35, JI Jend, Gatot Subroto No. 42, 12710, Jakarta, Indonesia*

[2]*Petroleum Geoscience Program, Chulalongkorn University, 254 Phayathai, Pathumwan, Bangkok, 10330, Thailand*

[3]*PTTEP (PTT Exploration and Production Public Company Limited), Soi 11, Vibhavadi-Rangsit Road, Chatuchak, 10900, Bangkok, Thailand*

[4]*Petroleum Geophysics Program, Department of Geological Sciences, Chiang Mai University, 239 Huay Kaew Road, Chiang Mai, 50200, Thailand*

ABSTRACT

The South Makassar Strait mass transport complex (MTC) covers an area of at least 9000 km^2 and has a total volume of 2438 km^3. It is composed of a shale-dominated sedimentary unit with high water content. Seismic reflection data across the South Makassar Strait MTC show that it displays relatively coherent internal sedimentary stratigraphy that in the toe region is deformed into well-defined thrust-related structures (imbricates, ramps and flats, fault bend folds). It is one of the largest known coherent MTCs. The bowl-shaped central core region is as much as 1.7 km thick, and is confined to the west and east by 355° and 325° trending (respectively) lateral ramps in the upper slope area that pass via oblique ramps into a northeast-southwest–trending frontal ramp area. The core area passes via the lateral, oblique, and frontal ramps into an extensive, thin (tens of meters thick) region of the MTC (the lateral and frontal apron areas) that are internally deformed by thrusts, normal faults, and thrust faults reactivated as normal faults. The MTC anatomy can be divided into extension headwall, translational, toe, flank, lateral apron, and frontal apron domains. The headwall region is located in the upper slope area of the Paternoster platform; the main body of the slide is in the deep-water region of the Makassar Strait. The complex is interpreted to be triggered by uplift of the platform area (accompanied by inversion), and/or basin subsidence, which caused seaward rotation of ~2° of the Paternoster platform in the Pliocene. Variable uplift promoted sliding dominantly from the eastern and western margins of the headwall. The internal fault patterns of the MTC show that extension in the upper slope to lower slope in the core area changes downslope to compressional structures in the toe domain and apron. Later extensional collapse of parts of the compressional toe area occurred with negative inversion on some faults. The coherent internal stratigraphy, and evidence for multiphase extension in the eastern headwall area, suggests that the ~6–7 km of shortening in the toe region of the MTC occurred at a slow strain rate. Therefore, this type of MTC does not have the potential to generate tsunamis.

INTRODUCTION

Since the Indonesian government conducted speculative two-dimensional (2D) seismic surveys in the eastern part of the deep-water Makassar Strait basin from 2001 to 2004, several oil and gas companies signed exploration contracts in 11 working areas. Significant activities include acquisition of more than 13,000 km of 2D, 12,000 km^2 of 3D seismic surveys, and 15 exploration wells. Data from the southern part of the Makassar Strait basin revealed a very extensive mass transport complex (MTC) in the upper part of the basin fill that covers an area of ~8985 km^2. Here we focus on describing the morphology of this giant relatively coherent MTC, and try to explain why it is characterized by large-scale internal deformation rather than disintegrating into smaller, more chaotic blocks. Water depths in which the MTC is found range from 1000 to 2000 m. The MTC covers the slope to basin floor area and the current seafloor morphology is probably similar to the paleomorphology when the MTC was deposited in the early Pliocene (Fig. 1).

Mass transport complex (MTC) is a general term used for an underwater landslide deposit that undergoes some combination of creeping, sliding, slumping, and/or plastic flow in a marine or freshwater lacustrine environment (e.g., Dott, 1963; Nardin et al., 1979; Moscardelli and Wood, 2008). Underwater landslides in a marine environment commonly occur around the slope area, in the transition zone between the shelf and deep-water areas. In recent years 2D, and particularly 3D, seismic data have enabled large MTCs to be described in considerable detail. Numerous kinematic indicators internal to large slides can be identified from seismic data (e.g., Bull et al., 2009) and can be seen in parts of the slide described here. The traditional classification systems for describing MTCs focus on sedimentary processes (e.g., Nardin et al., 1979). More recent classifications have defined the geological context of the slides by dividing them into shelf attached, slope attached, and detached systems (Moscardelli and Wood, 2008), or focus on the magnitude of translation (Frey-Martinez et al., 2006). Two end members of MTC translation were identified by Frey-Martinez et al. (2006) as (1) frontally restricted MTCs where translation is limited and the slide does not overrun the undeformed downslope strata, and (2) frontally emergent, where the slide ramps up from its basal shear surface and overruns the seafloor in an unconfined fashion. The South Makassar Strait MTC discussed herein is in the slope-attached category of Moscardelli and Wood (2008), and is closer to the frontally restricted than the frontally emergent end member of Frey-Martinez et al. (2006).

In a deep-water environment, MTCs, products of mass transportation processes, often dominate the basin stratigraphy, and are intercalated

*Formerly at Chulalongkorn University.

†Present address: 1107 Green Valley Drive, Houston, Texas 77055, USA.

Geosphere; April 2015; v. 11; no. 2; doi:10.1130/GES01077.1; 27 figures; 1 table.

Received 9 May 2014 ♦ Revision received 26 November 2014 ♦ Accepted 8 January 2015

with turbidite deposits (Dykstra et al., 2011). MTCs are commonly large enough to be geohazards, and the largest can be tsunamigenic (e.g., Watts, 1998, 2003; Wright and Rathje, 2003; Mosher et al., 2010; Yamada et al., 2011). MTCs became of interest to oil and gas exploration and development when wells and facilities were placed in deep-water environments (Shipp et al., 2004; Mosher et al., 2010; Yamada et al., 2011). On a worldwide basis, 90% of MTC's are mud prone (Meckel, 2011), but a few provide commercial reservoirs for hydrocarbons. As an example, the reservoir in the nearby Ruby Field (Fig. 1) in the Makassar Strait (Tanos et al., 2012; Pireno and Darussalam, 2010) is an MTC deposit with a predominantly carbonate facies.

REGIONAL GEOLOGY

The study area is in the southern Makassar Strait between the Paternoster platform on the eastern margin of Borneo to the west and the West Sulawesi fold belt to the east (Figs. 1–3). It is generally accepted that the Makassar Strait basins were formed as result of a broad zone of extension that continues onshore in the Kalimantan region of Borneo and in western Sulawesi (e.g., Cloke et al., 1997, 1999; Calvert and Hall, 2003). The onset of rifting was pre–45 Ma in the North Makassar Strait basin, and possibly slightly younger in the South Makassar Strait basin around the early-middle Eocene (Bachtiar et al., 2013; Kupecz et al., 2013). The younger basins initiated during the middle Eocene are exposed onshore (Bachtiar et al., 2013). The majority of the deep-water rift subbasins in the Makassar Strait are sealed by early Oligocene postrift sediments. However, on the western margin of the deep-water area on the Paternoster platform, extension appears to have continued on some faults into the Oligocene, and possibly into the late Oligocene–early Miocene (Kupecz et al., 2013). Despite this local evidence for relatively late extensional activity, much of the Makassar Strait area has been undergoing postrift thermal subsidence since the Oligocene. The postrift subsidence may have been enhanced by flexural subsidence related to thrusting and inversion in the East Kalimantan

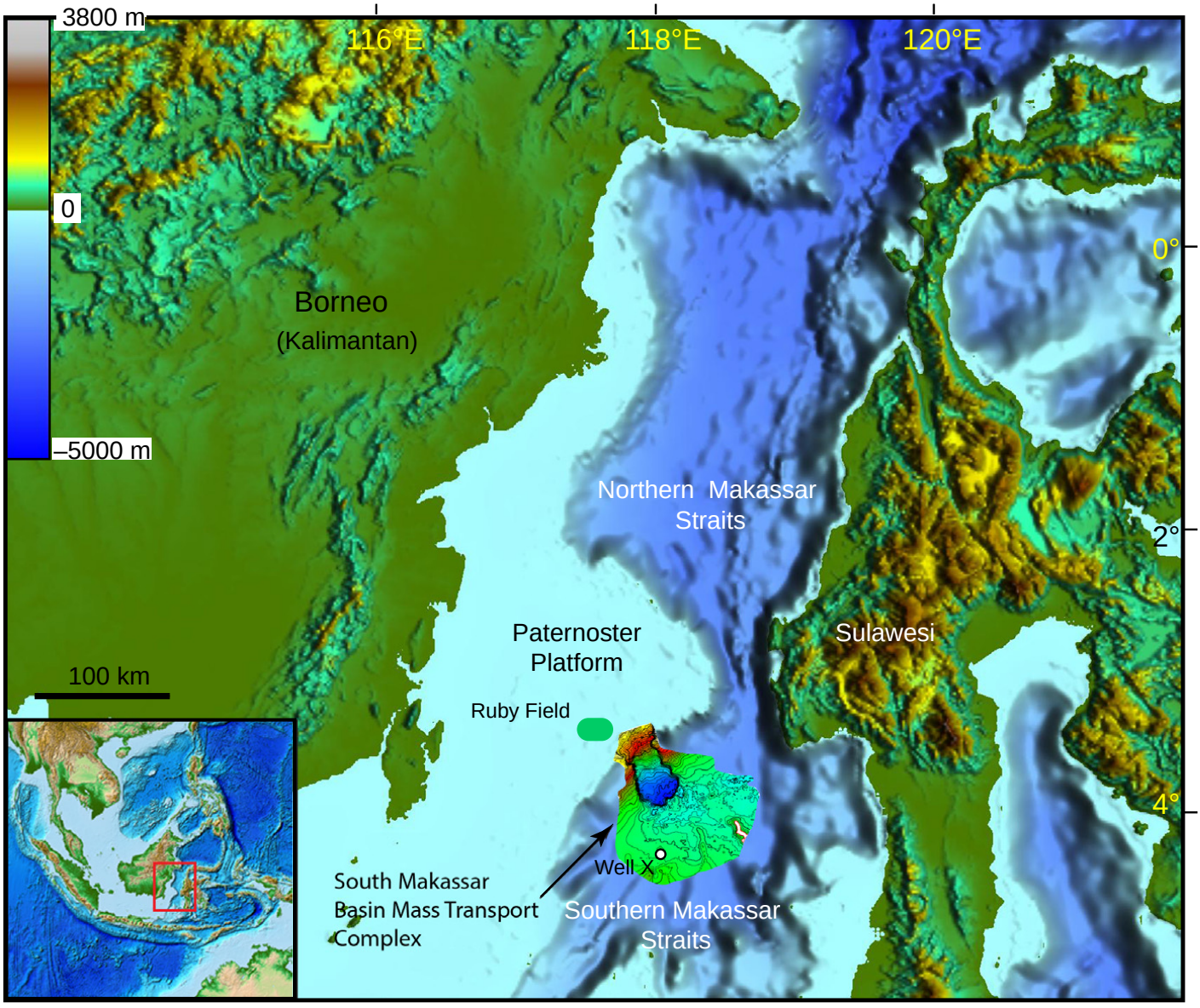

Figure 1. The South Makassar Strait mass transport complex.

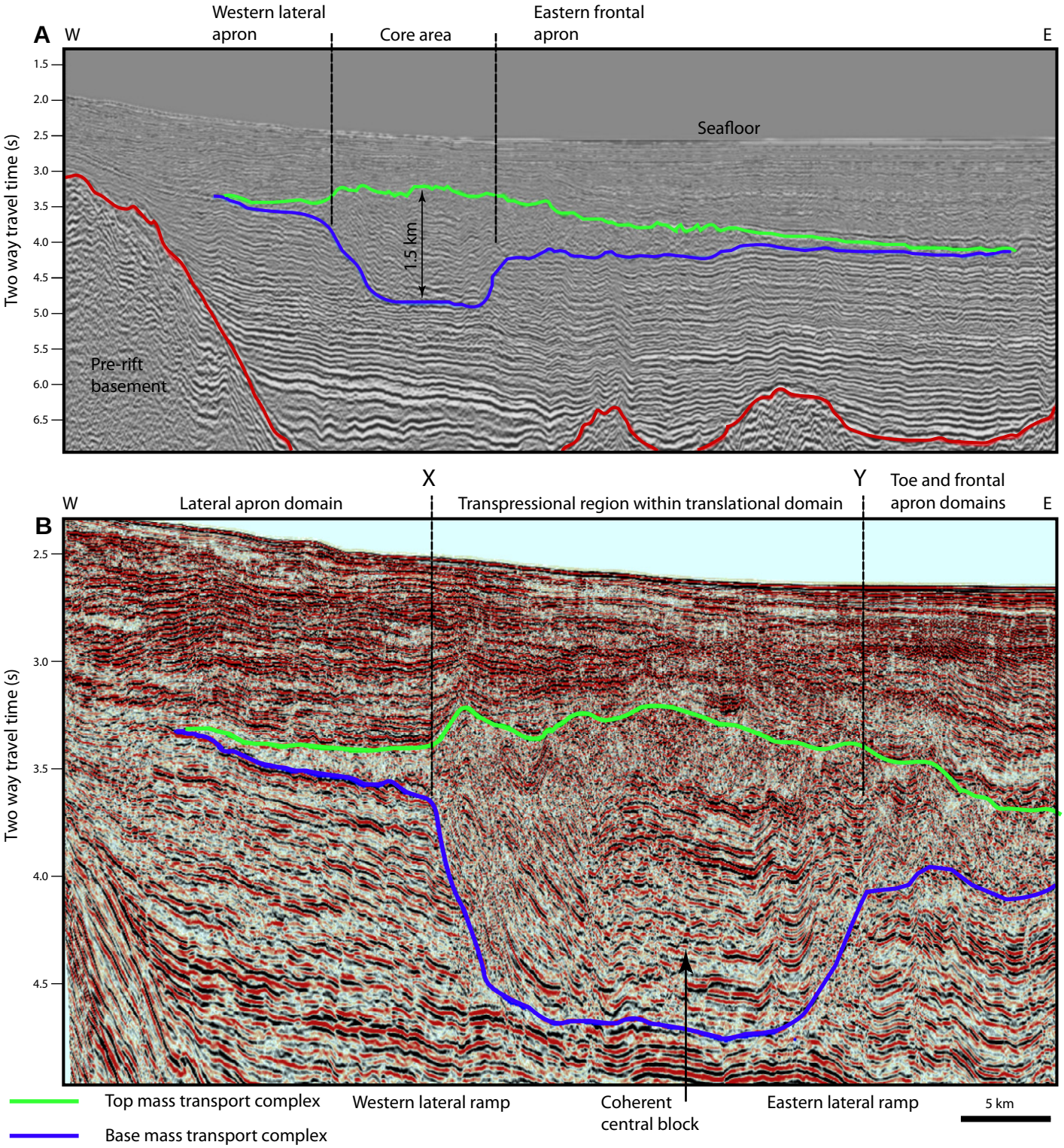

Figure 2. (A) East-west seismic line through the South Makassar Strait showing an oblique section through the mass transport complex (MTC) that is more oriented in the strike-direction than the dip direction. The section crosses two major lateral ramps that thin the MTC considerably from its 1.5 km thickness (indicated). Seismic section is vertically exaggerated (>10:1). (B) Detail of transverse seismic section through the translational domain of the core area. X—western lateral ramp; Y—eastern lateral ramp.

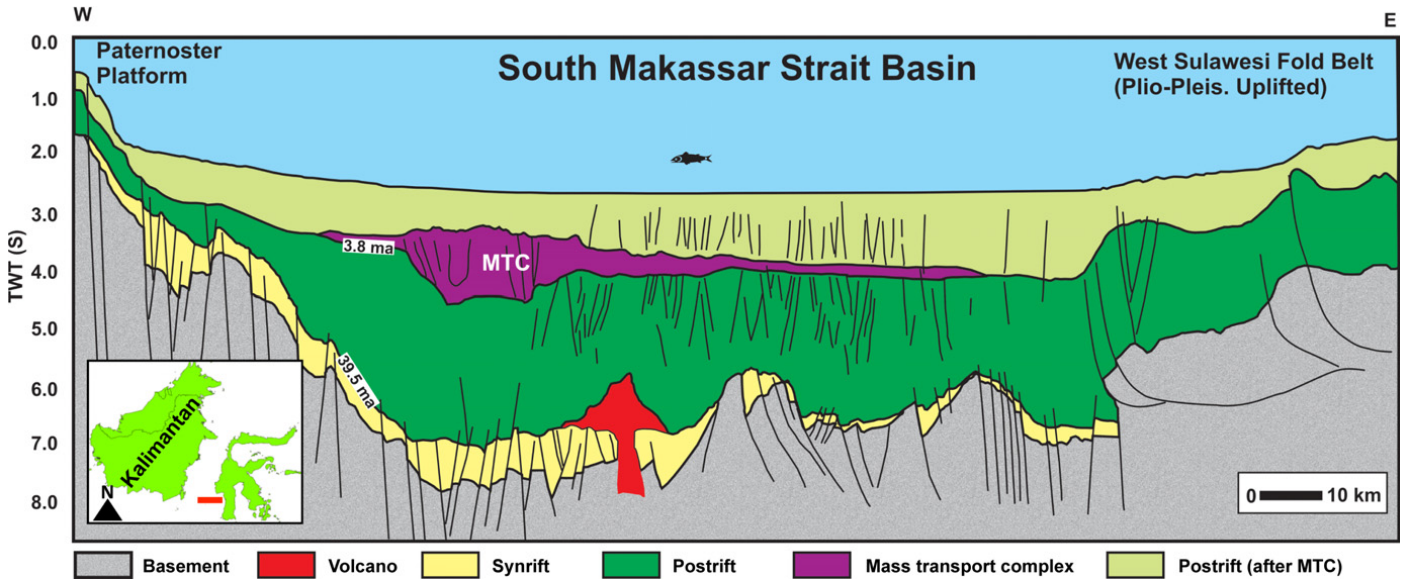

Figure 3. East-west cross section through the South Makassar Strait mass transport complex (MTC) illustrating the main Cenozoic features of the basin based on seismic and well data. TWT—two-way traveltime; Kalimantan—Borneo; Plio-Pleis.—Pliocene–Pleistocene. Modified from Armandita et al. (2011).

region of Borneo since the early Miocene and in the western Sulawesi area since the early Pliocene (Satyana, 2010). A generalized cross section of the basin is shown in Figure 3. The Makassar MTC occurs high in the section during the postrift subsidence phase (Fig. 3). The slide originated within latest Miocene to early Pliocene section on the northeast-southwest–trending slope of the Paternoster platform, and covers a substantial portion (~9000 km^2) of the South Makassar Strait deep-water area (Fig. 1).

WELL CORRELATION TO THE MTC

Well X penetrated the outer part (apron) of the MTC body (Fig. 4). Based on micropaleontology results from well X (Fig. 5), the sediments that were incorporated into the South Makassar Strait MTC were deposited during the latest Miocene to early Pliocene.

The operator provided a tie of the well to the seismic data. Although well X did not penetrate the core area of the MTC, the mostly undeformed strata outside of the MTC in the well area can be clearly correlated on seismic reflection data to the reflective strata within the thickest part of the MTC (Fig. 4). The MTC strata are equivalent to the Dahor Formation in the western part of research area, in the Paternoster platform (Fig. 5). The projected deepest MTC basal detachment level into well X corresponds with the boundary between two different sedimentary units (Fig. 5). Unit 2 above 2900 m exhibits relatively lower gamma ray, and higher resistivity, values compared with the lower part of the unit. This change corresponds with the actual base of the thin MTC encountered in the well. The Dahor Formation (late Miocene–Pleistocene) is composed of deep-water shales, with thin silty turbidites and allodapic limestones, while the upper Warukin Formation (late Miocene) displays less silty beds and more carbonates. The Dahor Formation contains a number of relatively small MTCs that are visible on seismic reflection data.

METHODOLOGY

The primary data sets used for this study are 2185 km^2 of 3D and 7054 km of 2D seismic reflection data and 1 well. The seismic reflection data set covers ~11,000 km^2 area of the South Makassar Strait basin. In the headwall area the dominant frequency of the 3D seismic in the zone of the MTC is ~30 Hz, while for the 2D seismic it is ~17 Hz. Assuming vertical resolution is ¼ wavelength, and an interval velocity of 2000 m/s, then the vertical resolution is ~29 m for the 2D seismic and 17 m for the 3D seismic data.

Structural mapping over the area using 2D and 3D seismic reflection data defined the base and top of the main MTC body. The main features of the body could be defined in 2D seismic data, but the details regarding internal fault orientations, internal stratigraphy, and geometry of the headwall area were defined from 3D seismic reflection data. The 3D seismic data cover two areas: the headwall region, and the region of the southeast oblique ramp region of the central core area (Fig. 6B). Fault complexes were mapped in the toe domain in the western part of the central 3D seismic block. The fault complex was mapped based on correlation of inlines (east-west), crosslines (north-south), and where necessary arbitrary lines with a range of orientations. Root mean square (RMS) and time-amplitude slice maps were also used to confirm the faults and other detachment surfaces within the main body of the MTC. Similarity cubes were made for the 3D seismic data sets, but the reflectivity within the MTC is too variable in continuity to generate good images. Correlations of faults were made from standard mapping of vertical section lines that match with structure trends shown by the amplitude time-slice maps. Horizons were mapped locally within coherent parts of the slide using inline and crossline spacing of 20 lines, and in places at closer spacing (5 and 10 lines) in areas of high complexity. The regional extent and geometry of the South Makassar Strait MTC was defined by mapping the top and base of the body in 2D and 3D seismic data (e.g., Figs. 6 and 7).

Depth conversion was based on the tie of well X to seismic data provided by the operator. Sonic data from the well only cover the lower part of the interval from the seafloor to the base of the section that is involved with the main part of the slide. Based on the seismic correlation and the thickness of the interval in the well, the average velocity from the seabed to the top of the MTC is 1498 m/s. This very slow velocity indicates that a high percentage of water is present in shallow subsurface deep-water sediments. However, it

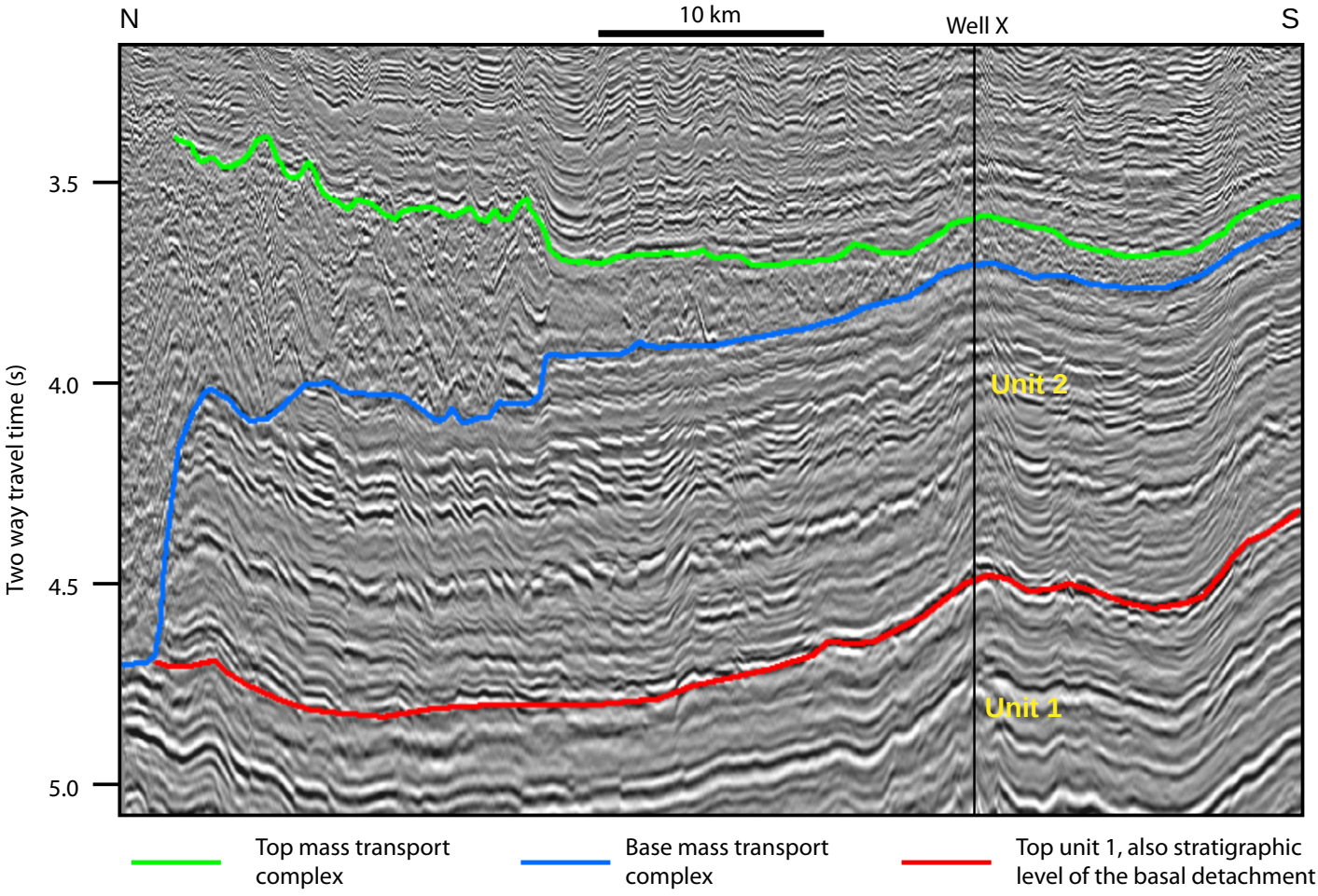

Figure 4. North-south two-dimensional seismic section through the South Makassar Strait mass transport complex (MTC). This section is oblique to the regional strike and dip of the MTC, but is more in the dip direction than the strike direction. The MTC shows one major and two minor ramps at its base. The section shows that well X is located at the thin, downdip part of the MTC. The frequent steep breaks in the seismic data outside of the MTC are due to polygonal faults. For well location, see Figure 1. CF—central area.

also suggests potential problems with the well tie, since typical velocities for such an interval are expected to be ~1600–1800 m/s. The seismic to well tie of the operator indicates that the interval between the basal detachment level and top of the MTC has an average velocity of ~2000 m/s (the interval between 3.6 s two-way traveltime, TWTT, and 4.5 s TWTT corresponds with depths of 2690 m and 3593 m respectively; i.e., an interval 903 m thick is equivalent to ~0.9 s TWTT). However, the partial coverage of the interval by the well sonic log indicates that a more appropriate average velocity would be ~1850–1900 m/s. It is well established within the petroleum industry that there can be issues with matching velocities from well log data to seismic data due to problems such as borehole rugosity. Unfortunately, we did not have access to the detailed well log information, so it is not certain that the well velocity data are better options than the velocity derived from the operators well to seismic tie. The slow velocities in the range of 1500–2000 m/s are reasonable, but may be limited to a narrower range if more complete sonic data were available. For consistency of data we used the velocities derived from the operators well to seismic tie, and anticipate the potential error margin between different methods is likely to be ~+10% for the upper interval (velocities should not be slower than water) and –10% for the MTC interval (the estimate used is likely to be on the high side).

GEOMETRY OF THE MTC

General Characteristics

The MTC covers an area of at least 9000 km^2 (Figs. 7 and 8). Its overall dimensions are 120 km in the north-northwest–south-southeast transport direction; it is as wide as 100 km. The isopach map derived from the top and basal horizons (Fig. 8) indicates that the total volume of the MTC is 2438 km^3.

The thickest part of the MTC forms the bowl-shaped core area that is as thick as 1.7 km (Fig. 8). The core is restricted to a region of ~930 km^2, subdivided into the typical MTC domains of the headwall, extensional, translational, and toe (contractional) domains. The basal detachment ramps up along lateral, oblique, and frontal ramps bounding the core area, and cuts out section within the MTC. Beyond the core area are the extensive lateral and frontal apron areas where the MTC is much thinner (generally tens of meters thick). Thinning of the apron area from the regions of the ramping basal detachment to the termination of the MTC has produced a low-taper wedge geometry (Fig. 7). The full extent of the MTC to the southwest and southeast is not known due to the absence of seismic data coverage, but in these areas the MTC is expected to be very thin.

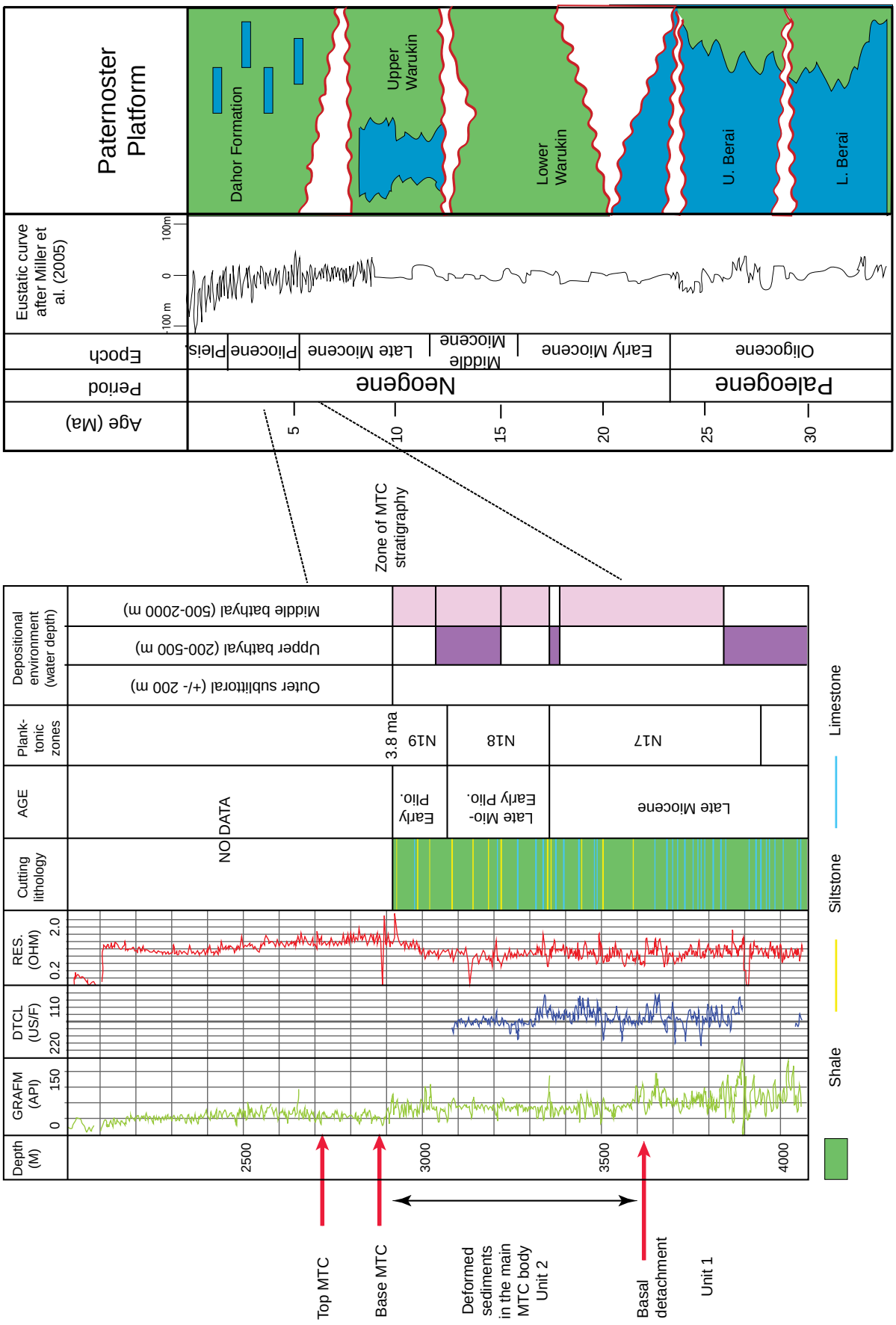

Figure 5. Stratigraphy of the South Makassar Strait, showing the segment of well X that crosses the interval of the mass transport complex (MTC). See Figure 6 for well location. Mio.—Miocene; Plio.—Pliocene; Pleis.—Pleistocene; U.—upper; L.—lower.

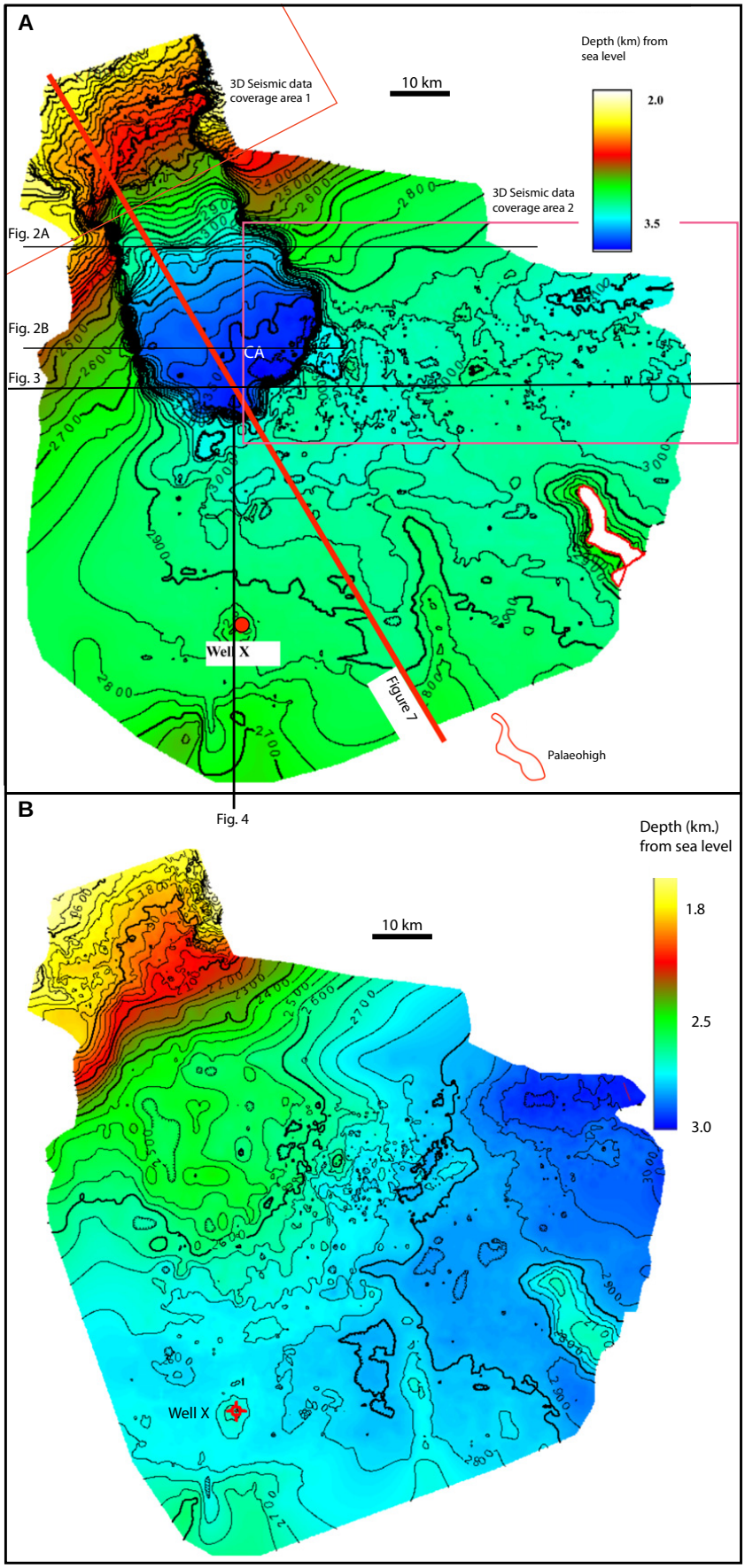

Figure 6. (A) Depth-structure map to base of the South Makassar Strait mass transport complex (MTC). 3D—three dimensional. (B) Depth-structure map to top of the South Makassar Strait MTC.

Terminology of Blocks

The use of the descriptor block is briefly reviewed here, because the term is widely used in the context of MTCs, but can actually refer to features with considerably different origins. The variations in part reflect the wide range of MTC geometries, which can range from internally chaotic bodies to coherent slides with well-preserved internal stratigraphy (e.g., Dott, 1963; Nardin et al., 1979). Within the chaotic bodies isolated blocks of lithologies different from the matrix are commonly present. These blocks may be internally highly contorted or little deformed, which can be due to different deformation mechanisms within the MTC, lithology, or degree of lithification (e.g., Frey-Martinez et al., 2005). Other intact blocks can separate from the front of a slowing flow and move ahead of the flow to form outrunner blocks (Nissen et al., 1999). Rafted blocks display coherent internal stratigraphy, and developed by fragmentation into independent units followed by translation considerable distances (kilometers) within a more mobile debris flow. For example, hard, cohesive clay blocks were transported in a coarse sandy debris flow of the BIG'95 MTC (western Mediterranean Sea; Canals et al., 2000; Lastras et al., 2005). Remnant, in situ, or relict blocks are coherent blocks of undeformed sediment that have not been moved by the MTC, but are partially or completely surrounded by MTC deposits (e.g., Alves, 2010). The terms thrust fault block and normal fault block are used here to denote regions within the slide where the internal deformation has affected a coherent stratigraphic package, translation has not been sufficient to separate and isolate the blocks, and hanging-wall and footwall cutoffs can be identified between the blocks. The 3D seismic data have permitted the identification of a number of MTCs with regions that display regular internal deformation with numerous thrust and normal fault blocks (e.g., Frey-Martinez et al., 2006; Silva et al., 2010; Ireland et al., 2011).

Extensional Domain

The most updip part of the extensional domain is the region of the headwall, which is located in the north-northwest area of the MTC body and is covered by 3D seismic data set 1

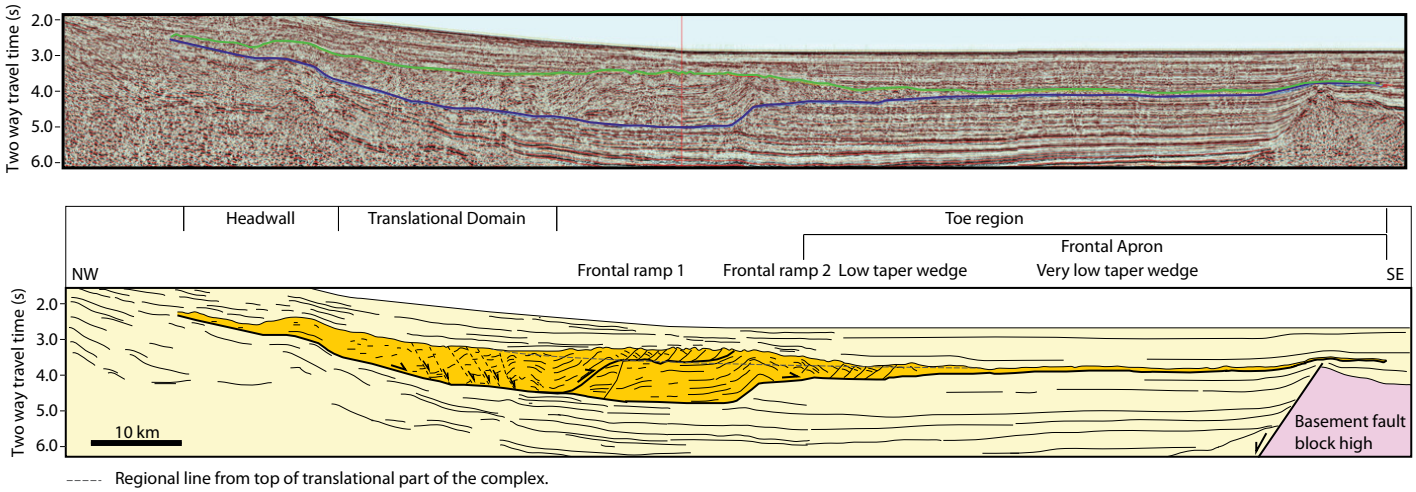

Figure 7. (A) Regional northwest-southeast–trending seismic line, one of the few regional lines approximately in the transport direction through the mass transport complex (MTC). (B) Region section through the South Makassar Strait MTC based on seismic line shown in A. See Figure 8 for location.

Figure 8. Depth-isopach map for the South Makassar Strait mass transport complex (MTC).

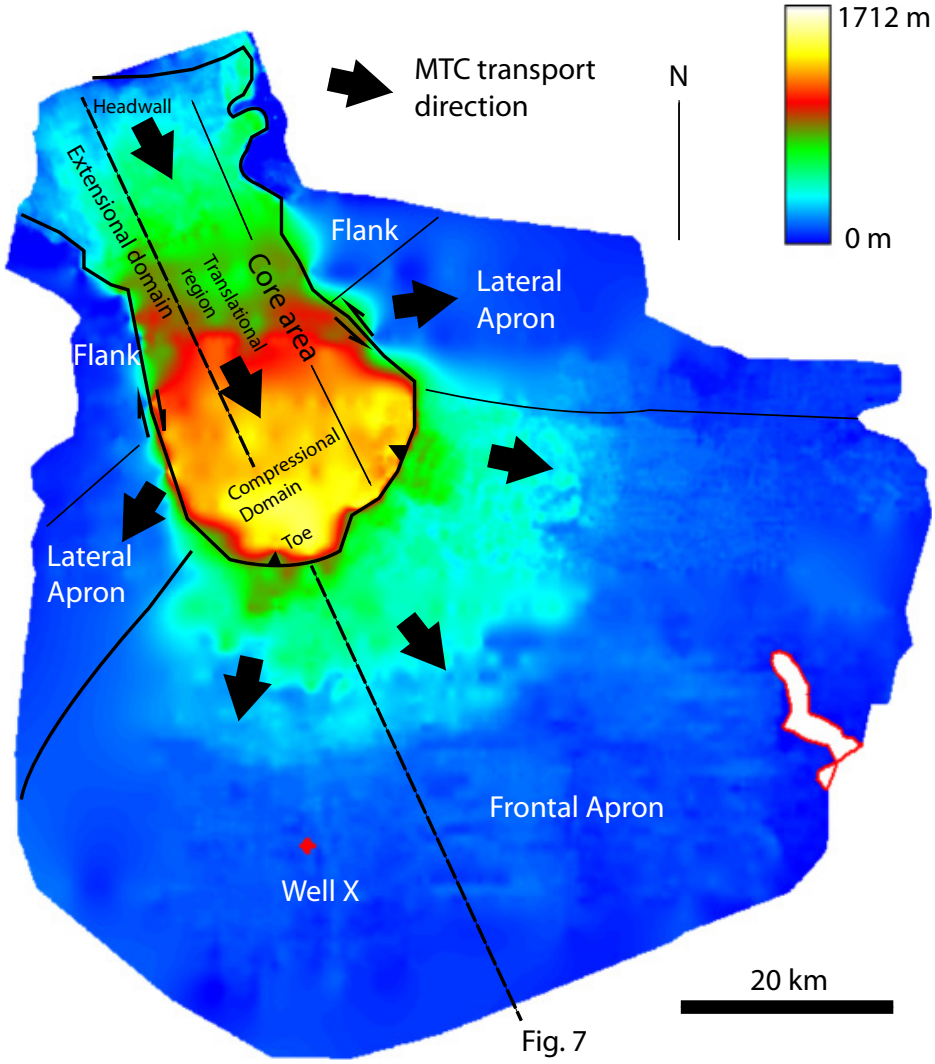

(Fig. 6B). The translational domain is farther downdip and less well imaged. In the headwall area the basal slip surface is gently inclined (4.6°) to the southeast (Fig. 9). The basal surface remains subparallel to bedding reflections in the footwall over much of the headwall area, and cuts upsection in a narrow zone ~3 km wide (Fig. 9). This gentle scarp is different in comparison with published MTC anatomy models (e.g., Bull et al., 2009) that show a steep scarp that dips in the range of 15°–35°. The one area where the basal fault exhibits steeper dips is along the eastern margin of the headwall (Fig. 9B), where the main bounding fault dips ~47°.

The region of the head scarp and depletion zone (sensu Frey-Martinez et al., 2006) is ~35 km wide (northeast-southwest) and 25 km long (northwest-southeast). Internally much of the MTC in the headwall area displays coherent reflections, but these are of variable character and extent. Figure 10B shows an amplitude extraction from a horizon slice that was made through the center of the complex. The most frequent strike directions of reflections are north-south to northwest-southeast and northeast-southwest. Different parts of the headwall area exhibit different internal reflection geometries. These areas are mapped in Figure 10A and illustrated in Figures 11–14. The limits of the areas are approximate because the boundaries are

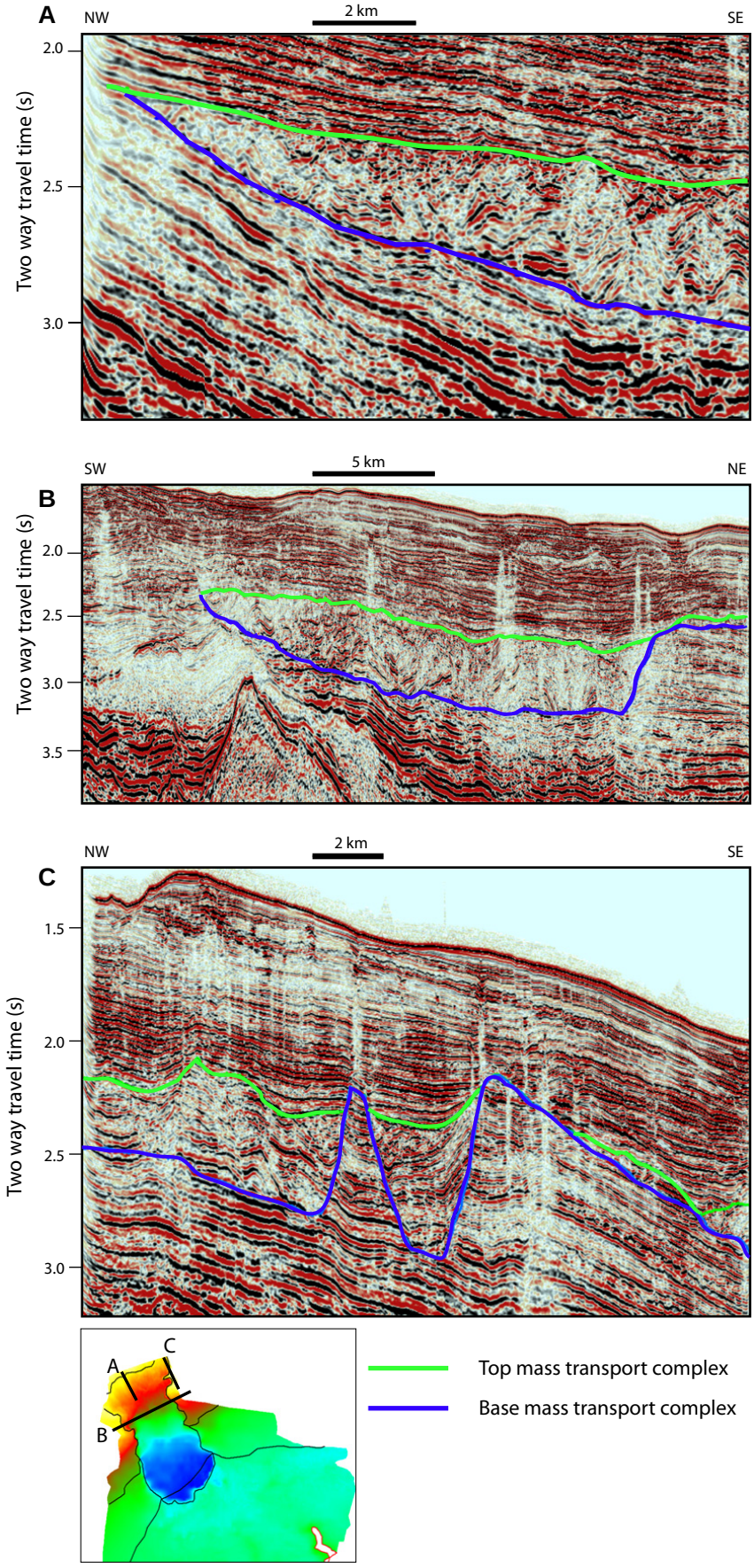

Figure 9. (A) Three-dimensional (3D) seismic line showing the characteristics of the headwall region of the South Makassar Strait mass transport complex. Although somewhat chaotic, the patterns of blocks rotated by normal faults can be discerned. (B) Strike 3D seismic section through the headwall area. (C) Arbitrary line in an approximate strike direction, eastern headwall area. See Figure 10 for location.

generally gradational. The characteristics of the areas are described as follows.

1. At the narrow taper updip end of the complex reflectivity is moderate to poor (Fig. 10). There are frequent discontinuous reflections that dip in the direction opposite to that of the basal detachment, suggestive of extensional rotated blocks. Correlation of horizons across blocks is difficult.

2. The updip wedge characteristics are similar to 1, but additional complexity is present in that the stratigraphy involved in the South Makassar Strait MTC is actually composed of several MTCs. In some areas over a distance of several kilometers, a clear depositional boundary between stacked MTCs can be identified (Fig. 11B). However, in other areas the boundary is broken up by internal faulting that is sealed by the top of South Makassar MTC reflection (Fig. 11A). These relationships are seen only in the southwest part of the complex (Fig. 10A).

3, 4, 5. Areas 3–5 are where well-developed tilted fault blocks, in relatively thick, coherent sections, are developed (Fig. 10A). The reflectivity indicates that the tilted blocks with rollover anticlines strike predominantly north-south to northwest-southeast. Transport directions are primarily from west-northwest to east-southeast (3), northeast to southwest (4), and east to west (5). The southeast occurrence of 4 is marked by a change in transport direction from east to west at the headwall, to south-southeast at the downslope end (Fig. 10). The eastern margin of the headwall area is composed of two reentrants where north-south– to north-northwest–south-southeast–striking normal fault faults are present. Figure 9C shows a seismic line subparallel to the edge of the eastern margin where an undeformed (remnant or in situ) horst block lies between the two reentrants. Long (~9 km), narrow (to ~3 km wide) normal fault blocks subdivided by curved zones of strike-slip faults have rotated away from the eastern margin and progressively show reorientation with transport strikes between northwest-southeast to north-south near the headwall, to a more west-northwest–east-southeast direction

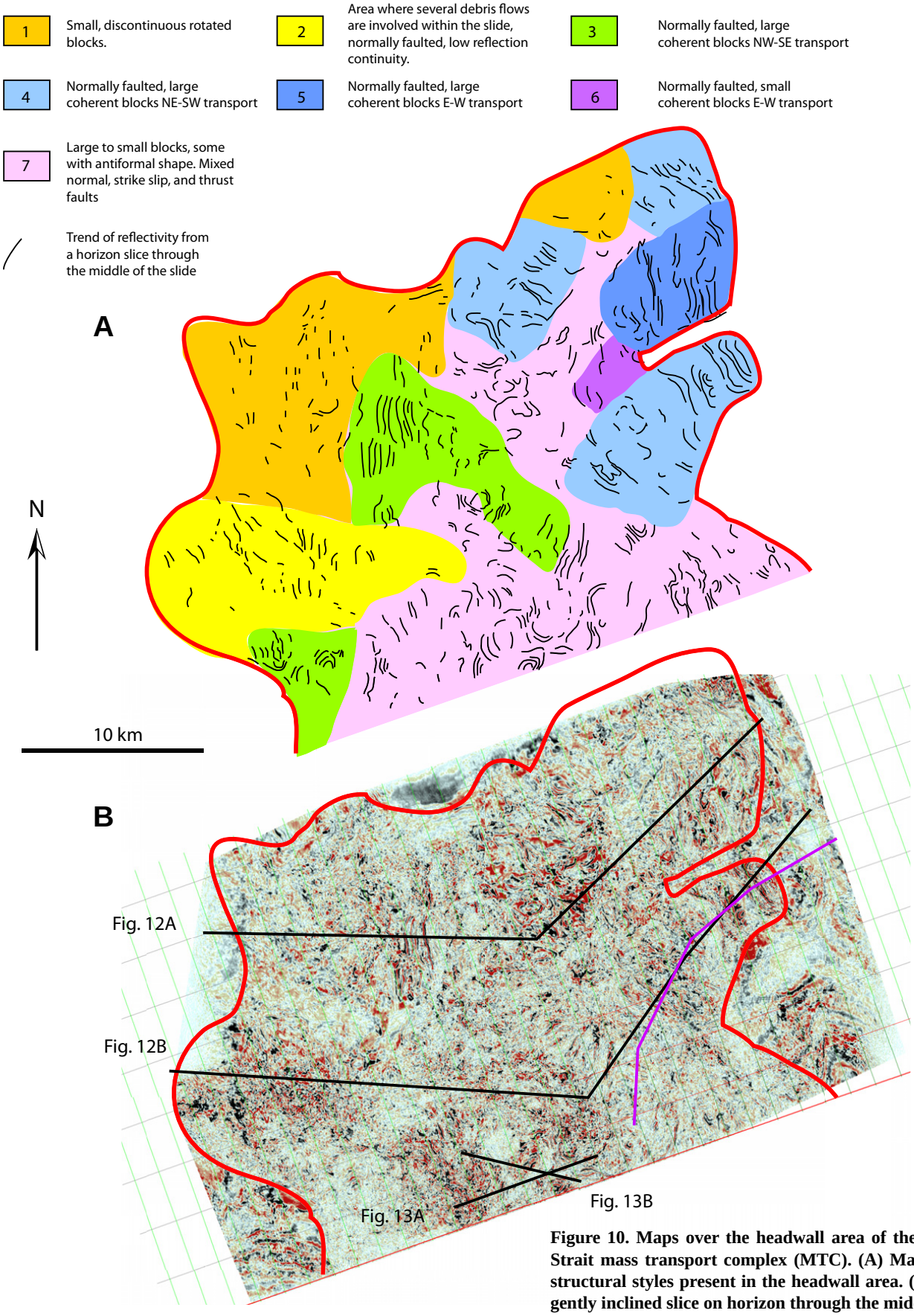

Figure 10. Maps over the headwall area of the South Makassar Strait mass transport complex (MTC). (A) Map of the different structural styles present in the headwall area. (B) Amplitudes on gently inclined slice on horizon through the middle of the MTC.

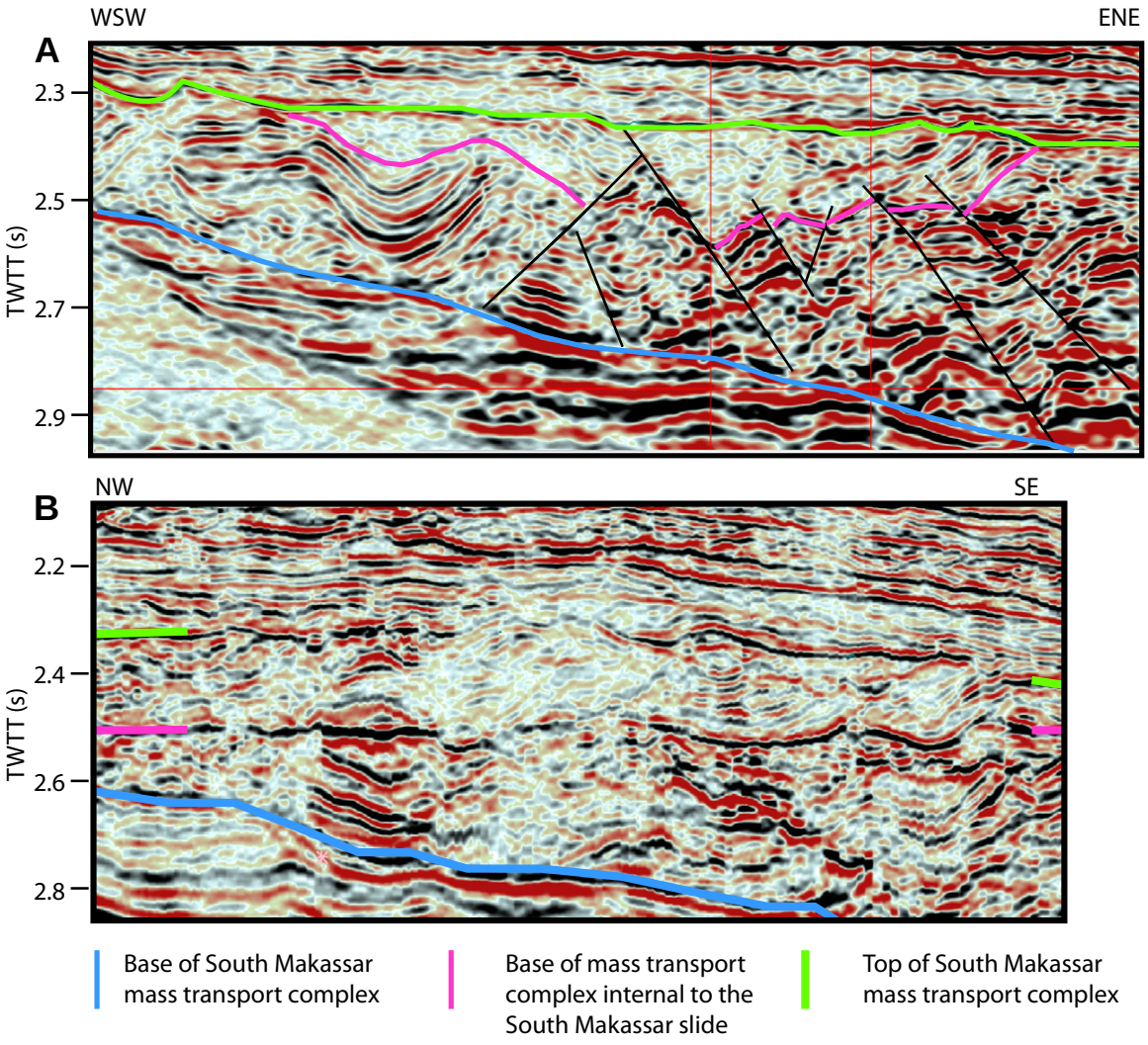

Figure 11. Seismic lines illustrating stacked mass transport complexes (MTCs) in the stratigraphy of the southwest part of the headwall area. See Figure 10B for location. TWTT—two-way traveltime. (A) Earlier deformed MTC overlain by later MTC (separated by magenta horizon), both offset by faults related to the South Makassar Strait MTC. (B) Seismic line showing largely undeformed contact (magenta horizon) between two MTCs.

approaching the main body of the MTC (Fig. 15). In the eastern area heaves on faults that offset an internally mappable horizon indicate a total of ~2.5 km extension on the large, seismically visible faults (Fig. 15), with individual faults showing as much as 700–1000 m heave. Thickness discrepancies between the rotated blocks and the undeformed footwall area of the slide indicate that some synkinematic or postkinematic infilling of the fault block morphology occurred before deposition of the top of mass transport reflection. In the eastern part of the headwall area, there are several stages to fault development (Figs. 12 and 14). Figure 14 shows several stages to faults in the headwall area; the red horizon (2) marks a minor unconformity with local angularity that seals some fault movement. Above horizon 2, unit A is rotated by large faults near the headwall, and there is expansion of section to the west. Unit B is a very locally confined unit that shows decreasing dips upward, and marks a period of rotation. The synkinematic section is as much as 200 m thick. The horizon that typically marks the top of the MTC (Fig. 14, horizon 4) is locally an angular unconformity with units A and B, and the overlying unit C onlaps two tilted fault blocks. However, offsets by faults of several hundred meters affect horizon 4, indicating local reactivation of the major faults in the eastern part of the slide.

6. This small area comprises tilted fault blocks that are similar in style to 5, but are thinner, smaller, and less continuous.

7. The irregularly shaped area in the center of the headwall area comprises a region of high to low reflectivity, with a mixture of structural styles that includes rotated extensional fault blocks, antiforms, and synforms (Fig. 13). In places high-angle, probably strike-slip faults are present, while in other areas thrusts are interpreted (Fig. 13).

In the translational region (Fig. 8), mostly imaged in 2D seismic reflection data, internal reflectivity is not well developed, although in parts of some lines there are indications of internal reflectivity and the presence of rotated coherent, north-northwest–dipping normal fault blocks. However, given the dominance of headwall structural style type 7 (see Fig. 10A) at the southern end of the headwall 3D area, it is

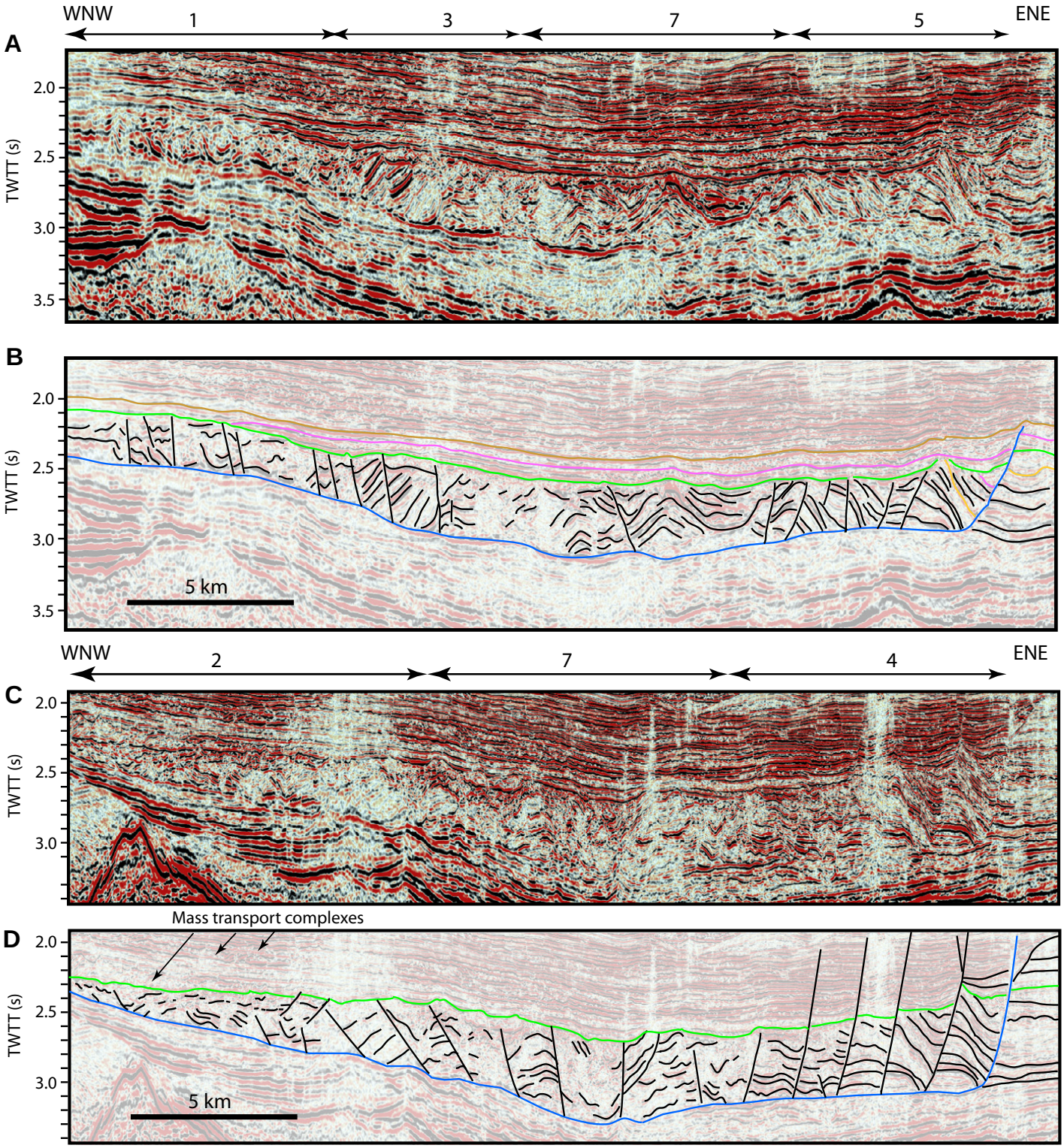

Figure 12. Regional lines across the headwall. TWTT—two-way traveltime. (A) Uninterpreted northern line. (B) Interpreted northern line. (C) Uninterpreted southern line. (D) Interpreted southern line. See Figure 10B for locations. 1, 2, 3, 4, 5, and 7 are the different structural style provinces shown in Figure 10A. Blue horizon—base of South Makassar mass transport complex (MTC), green horizon—top of South Makassar Strait MTC.

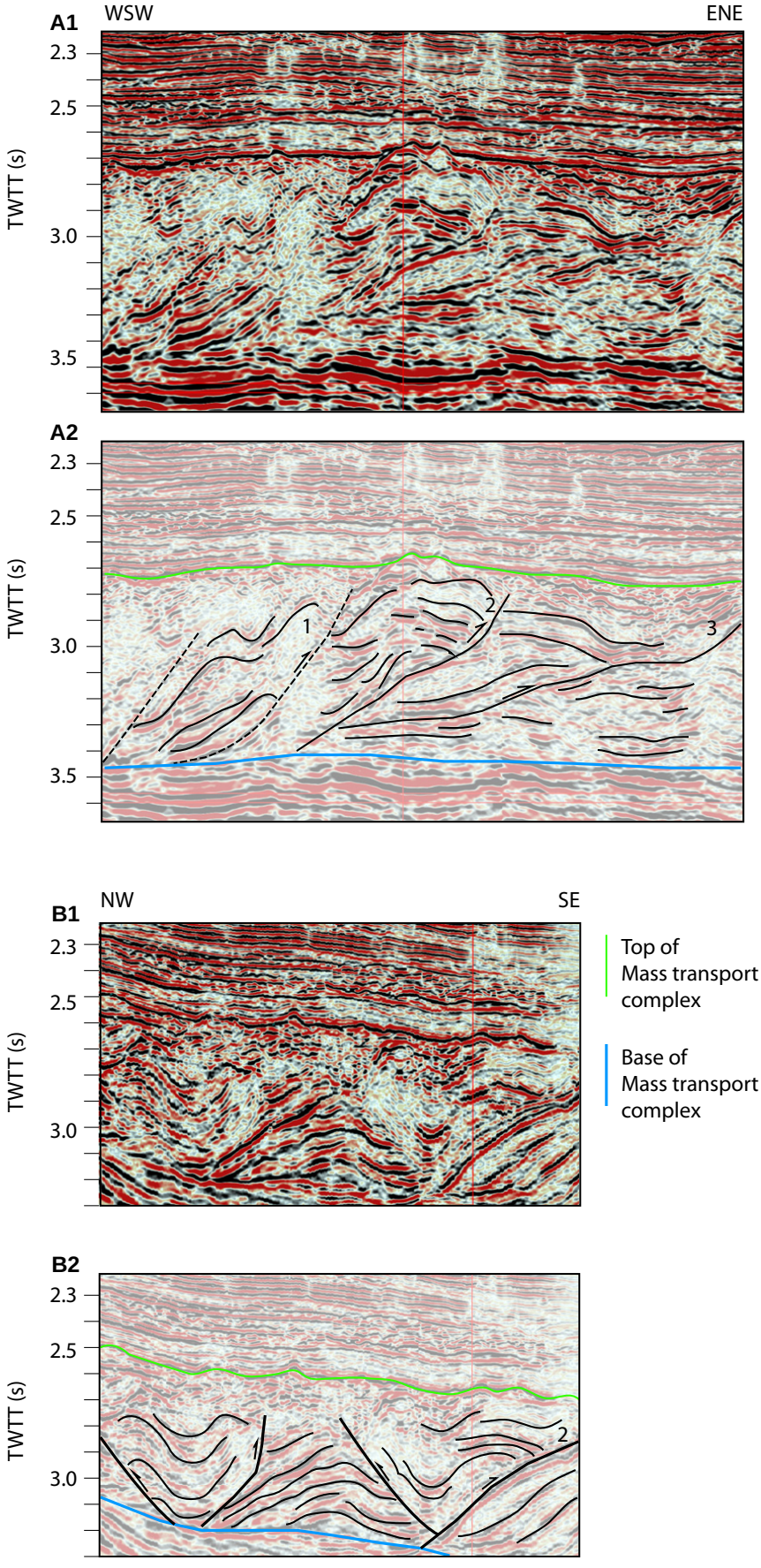

Figure 13. (A) 1—Uninterpreted east-west line through structural province 7. TWTT—two-way traveltime. 2—Interpreted line (see Fig. 10A). 1, 2, and 3 are thrust faults. (B) 1—Uninterpreted northwest-southeast line through structural province 7. 2—Interpreted line.

likely that this structural style dominates within the translational region. It is also possible that in places the seismic data are chaotic because the stratigraphic order has been lost and ductile deformation has started to dominate.

The translational domain (Fig. 8) is confined by east and west side lateral ramps from upper slope to the central core area and frontal ramps at the terminal and/or southeastward end of the central core. The higher parts of the east and west flanks have thin or no MTC section (Figs. 9B, 9C). The western and eastern lateral ramp areas exhibit different characteristics. The western lateral ramp strikes ~355°, dips ~25°–15° east, and has a vertical relief of ~1 km. There is very little westward translation of material (Fig. 2). In the center of the lateral ramp, there is no change of slope from the central core area to the lateral apron, indicating there has been little component of thrusting to the west up the ramp. The wedging of the section in the western apron as it decreases in thickness from 200 m to ~50 m in 9 km (east-west direction) is accomplished by the eastward dip (~1.9°) of the MTC base. The southern part of the western lateral apron remains narrow (~12 km) and the dip of the basal detachment decreases to ~0.5° east. The eastern lateral ramp trends 325°, exhibits dips between ~25° and 15° west, and has a vertical relief of ~650 m (Fig. 2). The difference in vertical relief of the lateral ramps between the two areas is accommodated in the northern and central part of the core area by ramps in the basal detachment that cut upsection ~180–250 m to the east. East of the eastern lateral ramp the basal detachment does not form a flat, but instead forms a very low-angle ramp that progressively cuts upsection by ~150 m over a distance of ~20 km. The eastern lateral apron area is more extensive than the western one, it extends as much as 30 km to the southeast, and decreases in thickness from ~400 m to 50 m, giving the wedge a taper angle of ~0.7°.

Contractional Toe Domain

About 20 km northwest of the frontal ramp 2 (Fig. 7B) and 35 km southeast of the headwall, the pattern of rotated normal fault blocks or chaotic zones that characterize the translational

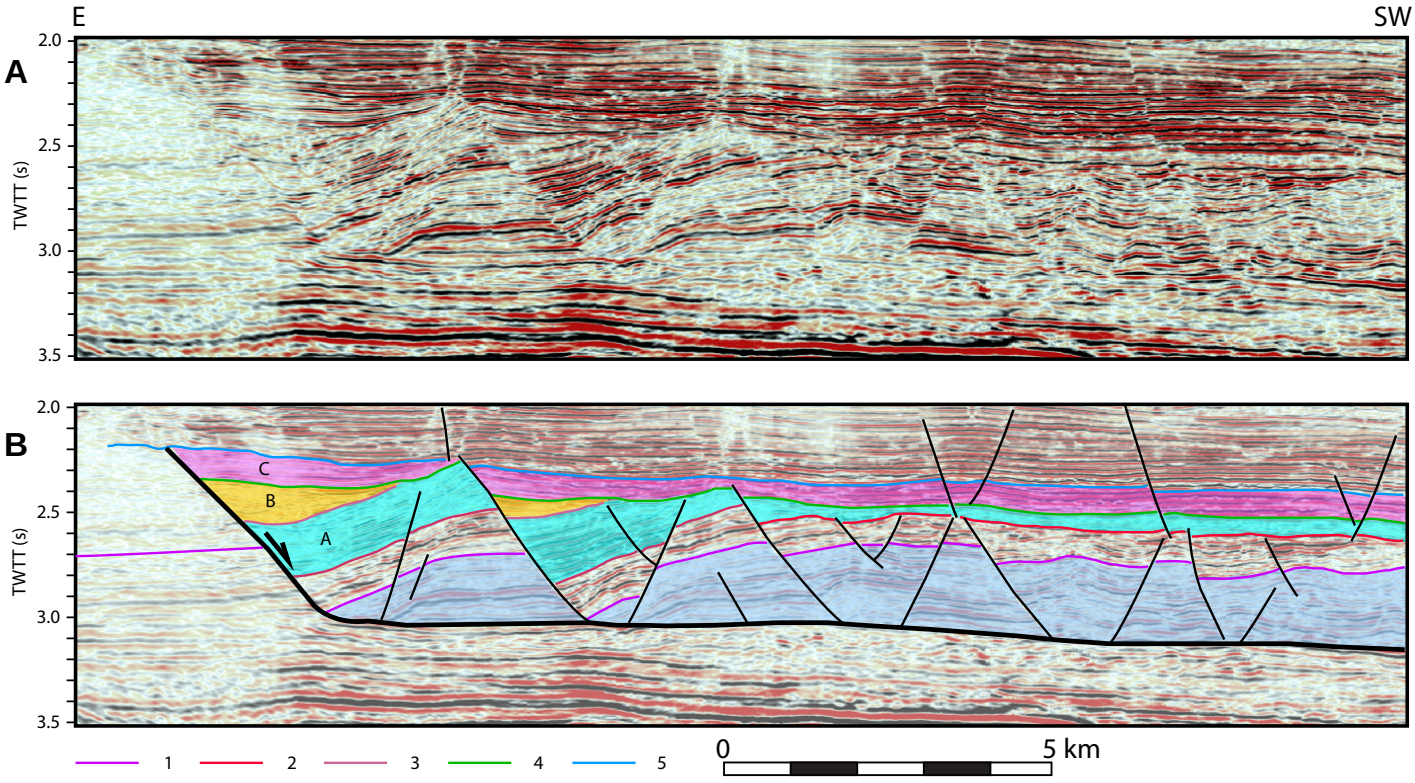

Figure 14. (A) Uninterpreted arbitrary line in an approximate transport direction, eastern headwall area. (B) Interpreted line. See Figure 10B for location. Horizons 1, 2, and 3 are horizons generally internal to the South Makassar mass transport complex (MTC); 4 is the top of the South Makassar Strait MTC, but in parts of the section horizon 4 has been affected by late movement of the MTC, and horizon 5 then locally marks the top of the mass transport activity. A, B, and C are different synkinematic layers.

domain changes in two main ways. The reflections become more coherent, and the top of the MTC becomes domed. When the top of the MTC in the extensional domain is projected downdip as a regional line, then the top of the MTC in the southern core area is seen to be elevated by as much as 300 m with respect to the regional line (Fig. 7B). The change in deformation style is marked by coherent reflectivity from sedimentary layers that are deformed by two major frontal footwall ramps, and associated fault bend folds (Figs. 7, 16, and 17). There is only minor, smaller scale internal deformation visible within the coherent thrust sheets. The biggest coherent block with subhorizontal reflections and little internal deformation is 1.20 km thick, 11.8 km long (northwest-southeast) (Fig. 2), and 10.7 km wide (northeast-southwest). The strata within the large block have reflection patterns that can be correlated with undeformed sediments west of the core area and below the lateral apron domain. One possibility is that such a coherent block is a remnant or in situ block and that the MTC has flowed around the block (e.g., Alves, 2010). However, this is not the case for the block in Figure 2, for the following reasons. (1) Figures 16 and 17 pass through the coherent block in Figure 2B. The location of the basal detachment as required by the frontal ramp (2; Figs. 16 and 17) is at the base of the coherent block in Figure 2B. (2) The section west and east of the block is also coherent, but more internally deformed; the difference between the two areas in Figure 2 is overemphasized by the strong vertical exaggeration inherent in trying to show the regional geometry of such an extensive MTC. (3) In Figure 2 the bases of the lateral ramps are also consistent with a detachment at the base of the coherent block.

Figure 16 shows part of a north-south–trending seismic line that is oblique to the transport direction, which gives an unusual perspective on some structures (such as the ramp–hanging-wall fold relationships, and thrust 1 that cuts downsection in the apparent transport direction in the southern part of the section). It is, however, one of the highest resolution lines and shows some key features. The two frontal ramps are present, with the most northern ramp (1) passing into a long flat region characterized by extensional collapse, with very clearly rotated blocks. Imbricate thrusts in the footwall of frontal ramp 1 offset the hanging-wall flat area of thrust 1. Figure 17 shows a seismic section across frontal ramp 2 in the transport direction (north-northwest–south-southeast); the fault bend fold in area c is complicated by extensional collapse. The top of the MTC is highly irregular, probably due to rotated tilted blocks (more clearly seen in Fig. 16) and local erosion and scouring. The overlying sediments onlap MTC top surface irregularities.

In the central and western parts of the core area the compressional zone is relatively simple, with two large ramps of the MTC. Passing eastward 3D seismic data show that the eastern side of the compressional zone is more complex, with several imbricate folds and thrusts being present in a zone 6 km long northwest of the main oblique ramp (vertical relief 600 m, dip 22° north-northwest; Fig. 18). Detailed mapping of the faults shows that the imbricate faults trend north-northeast–south-southwest to northeast-southwest and are cut by curved northwest-southeast– to east-northeast–west-southwest–trending strike-slip faults (Fig. 19). A detailed isopach map of the MTC in the southeast area shows the oblique ramp area on the southeast side of the core area. There is a smaller lobe of relatively thick MTC (predominantly in green) in Figure 20 that is east of the main oblique

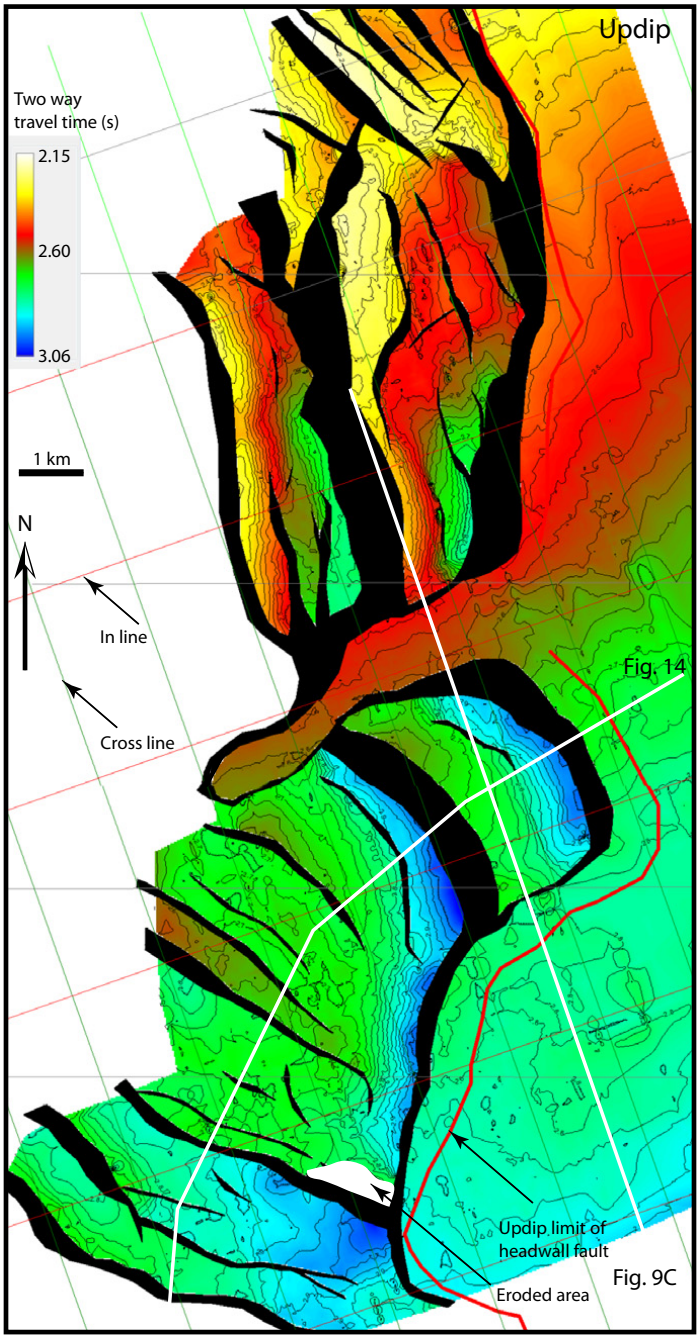

Figure 15. Time-structure map based on three-dimensional seismic data of the eastern headwall area on a horizon internal to the South Makassar Strait mass transport complex. The mapped horizon is horizon 1 in Figure 14B. TWTT—two-way traveltime.

ramp; this is because the thrust is deeper in the section in this area and ramps upsection to the northeast, southeast, and southwest. The fault pattern of the area is shown in Figure 20, along with an arbitrary 3D line showing the lateral ramp geometries.

Up the oblique and lateral ramps to the southeast and east, the region of imbricate thrusts grades into one where extensional rotated blocks dominate (Figs. 16, 17, 19, 21, 22). The main extensional faults define rotated blocks hundreds of meters wide, as much as 1 km wide and 300–400 m high, that form a zone as much as ~15 km wide east and southeast of the top of the oblique ramp (Figs. 19 and 20). Most of the extensional faults dip west to northwest toward the core area. Many of the imbricate thrusts also show evidence for negative inversion; the blue horizon in several imbricate stacks shows a normal sense of offset in Figure 18.

In the apron area the wedge decreases in thickness from ~800 m near the lateral, oblique, and frontal ramps, to ~50 m near its termination (where thin imbricated reflection patterns on seismic data cease). The distance from the start of the frontal ramp wedge to its southeastern termination is ~60 km. The decrease of the wedge thickness from 800 to 200 m occurs in ~20 km (i.e., an average slope of 1.7°), while the external wedge decreases from 200 to 50 m in 40 km (i.e., an average slope of 0.21°) (Fig. 22). The base is approximately flat, and the upper surface is dipping.

The extensive thin apron areas of the MTC are characterized by the inner belt of normal faults that dip toward the center of the MTC. The dip directions of the normal faults become more mixed outward (Figs. 21 and 22). Where the MTC becomes <100 m thick the internal character is not so easily discriminated, but generally the reflection character is regularly broken and gives the impression of compressional imbricates (Fig. 22); however, this may be a seismic resolution effect. The imbricate thrust systems are interpreted to be associated with compressional or pressure ridges (e.g., Nissen et al., 1999) with radial orientation, as seen on the RMS map (Fig. 23). These pressure ridges mostly correspond with the crests of folds related to the imbricate thrusts. The lobate frontal apron domain encompasses 58% of the total MTC area (Fig. 9). The basal MTC reflector in this domain shows unique and complex characteristics that can change abruptly from negative to positive amplitude and from one bed to the other. It is important to note that the basal surface of the MTC is not necessarily represented by a strong amplitude in a single bed, as reported in several previous studies (Bull et al., 2009; King et al., 2009). This basal detachment characteristic is interpreted as being caused by updip movement in the terminal part of the MTC, not as downdip movement involving sliding along a single detachment layer in the upper slope area of the MTC.

INTERPRETATION

The paleomorphology of the northeast-southwest–trending headwall domain is relatively similar to the recent morphology (bathymetry) above the MTC body at the edge of the Paternoster platform (Fig. 1). The morphological similarity indicates that the MTC was also formed in the slope area at the edge of the paleo-Paternoster high. Deposition of unit 2 (Fig. 5)

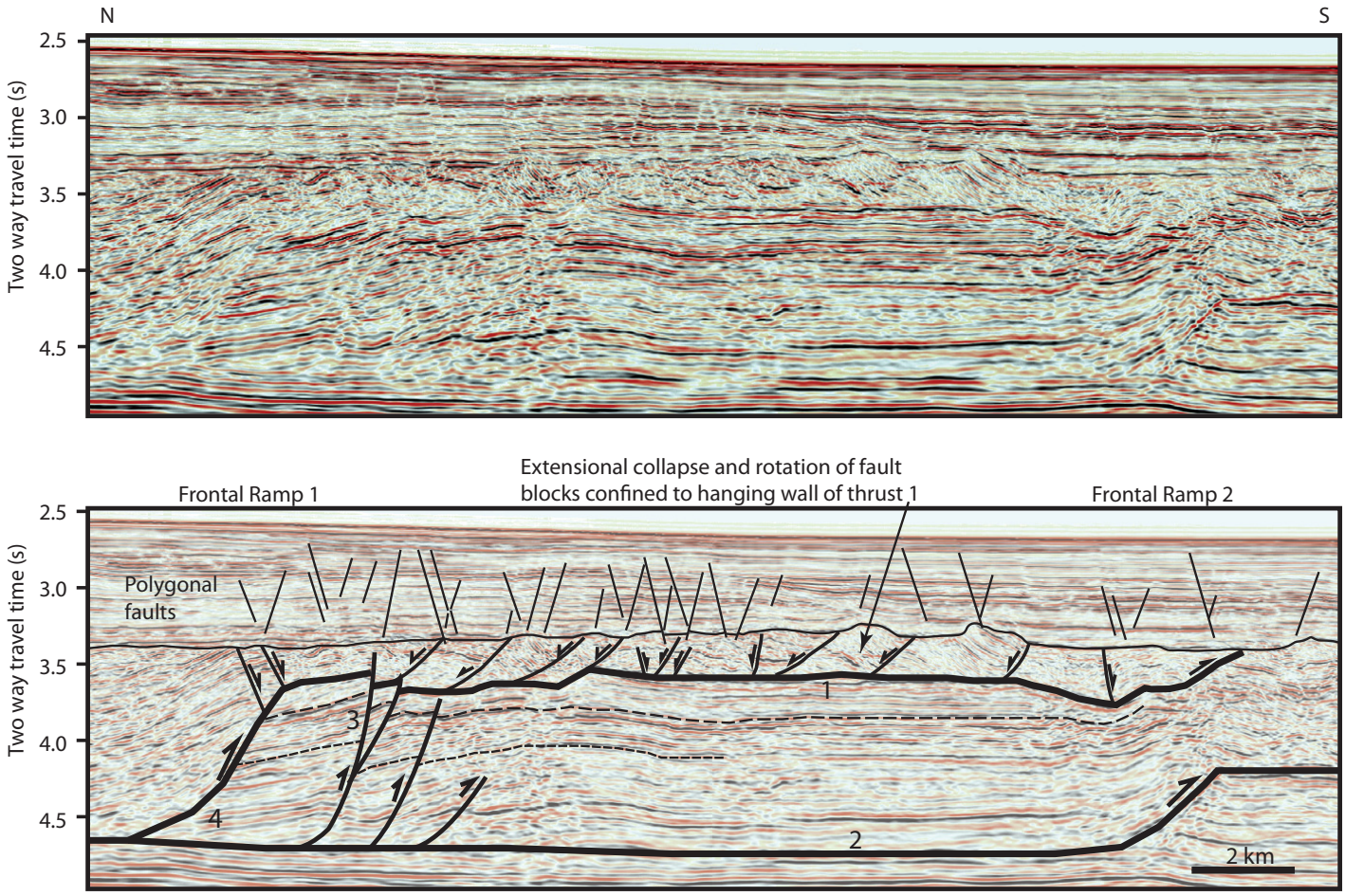

Figure 16. Two-dimensional seismic line (uninterpreted and interpreted) across the core area showing the coherent nature of the mass transport complex and the development of two major frontal ramps. 1—thrust, 2—basal thrust, 3—higher thrust (1) offset by imbricate thrusts from lower thrust (2), 4—basal thrust appears to locally cut downsection in the transport direction (possibly due to squeezing of unlithified sediment from the footwall of the ramp). See Figure 8 for location.

commenced in the late Miocene (ca. 6 Ma), coinciding with an initial period of uplift in the Paternoster platform (Tanos et al., 2012) and southern Kalimantan region of Borneo (Satyana and Armandita, 2008). The uplift process in eastern Borneo is probably still active; earthquakes associated with strike-slip and reverse faults have been recorded (Petersen et al., 2007). Uplift has also occurred in west Sulawesi since the early Pliocene (Nur'aini et al., 2005) and flexural subsidence may have caused the isostatic deepening due to loading on the west and east sides of the Makassar Strait (Satyana, 2010).

The difference of ~2° dip between post-MTC strata and pre-MTC strata (Figs. 7 and 9) indicates that the Paternoster platform underwent rotational uplift at the time of MTC formation. Based on biostratigraphy analysis at Well X, deepening of the South Makassar Strait basin from upper bathyal to middle bathyal (Fig. 5) occurred at a time similar to that of uplift of the Paternoster Platform. These uplift periods probably caused the instability and triggered major and minor MTC formation in the South Makassar Strait basin since the late Miocene. The South Makassar Strait MTC developed ca. 3.8 Ma (early Pliocene).

The dominance of northwest-southeast– to northeast-southwest–trending tilted blocks in the headwall area and overall areal distribution of structural style types (Fig. 10A) suggests that material was primarily derived from the northwest and northeast parts of the headscarp rather than from the north, and then has rotated about a vertical axis to join the overall south-southeast transport direction of the slide passing farther south. This observation suggests that uplift of the headwall area was focused on a north-northwest–south-southeast–trending axis (possibly related to inversion) that flanked the headwall area, rather than simply being from regional uplift to the north.

The sediments incorporated into the South Makassar Strait MTC on the eastern side of the headwall are predominantly well layered, continuous reflections, with a few minor interbedded MTCs. On the western side two or three larger MTCs are present and in places dominate the stratigraphy. Therefore, identification of deformation related to the South Makassar Strait MTC versus the earlier MTC emplacement becomes more difficult on the western side compared with the eastern side. Nevertheless, late faults (related to the South Makassar MTC) that cut though all the stacked MTCs can be identified in places.

The occurrence of normal faults, folds, thrusts, and strike-slip faults in structural style 7 (Figs. 10A, 12, and 13) of the headwall area is interpreted to be the result of extensional slides converging from different directions, causing a mixture of compressional and strike-slip deformation farther downslope in addition to mass

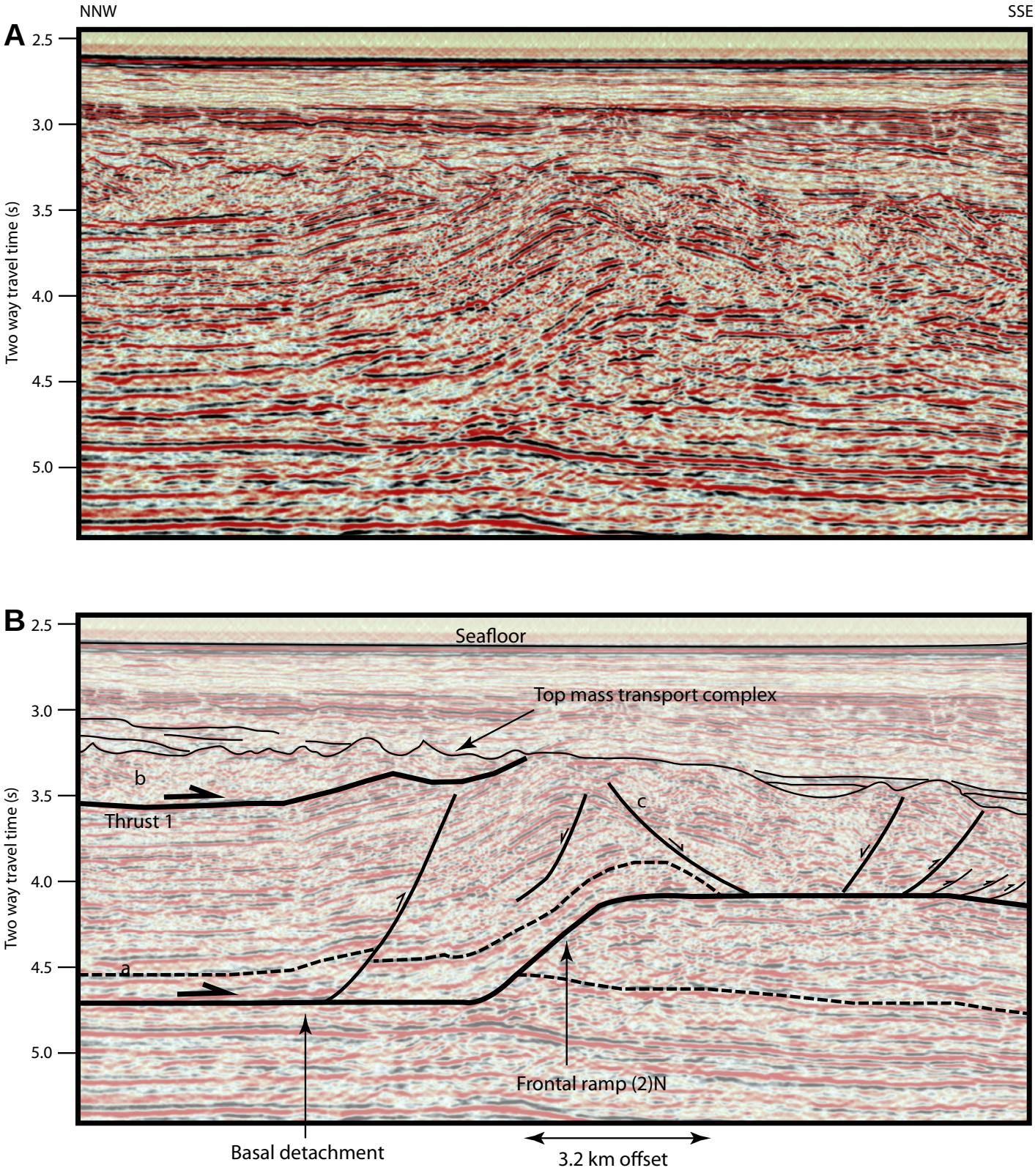

Figure 17. (A) Uninterpreted two-dimensional seismic line showing a major frontal ramp in a coherent part of the slide. (B) Interpreted seismic line. Frontal ramp: a—marker horizon, b—extensional collapse area in hanging wall of thrust 1 (see Fig. 16 for more regional context), c—extensional collapse in area of fault bend fold above frontal ramp 2. See Figure 8 for location.

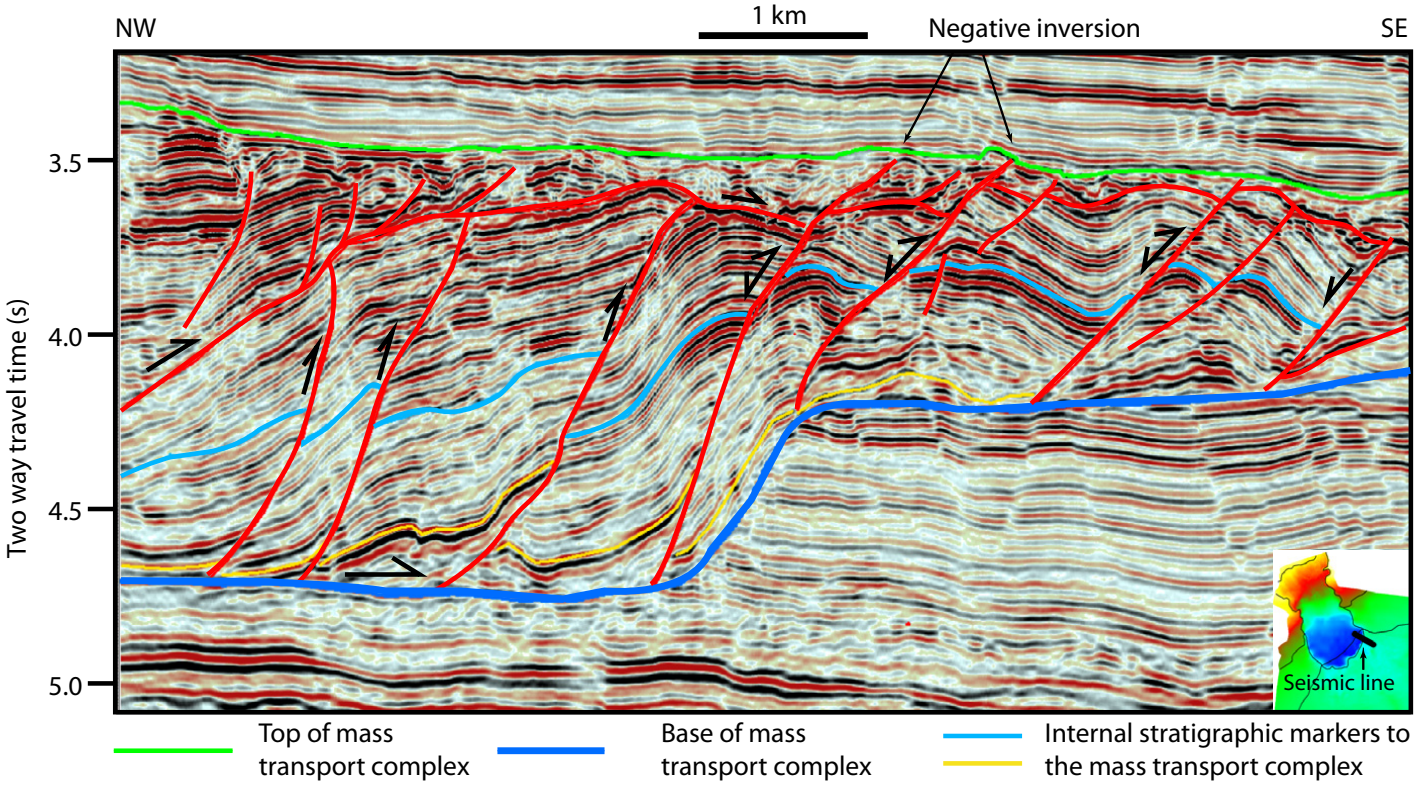

Figure 18. Northwest-southeast arbitrary line through three-dimensional seismic survey 2 (Fig. 6), showing the oblique ramp area on the eastern margin of the core area. The imbricate thrusts are present west of the main basal thrust ramp. Later extensional collapse has affected the southeast part of the line. See Figure 19 for location. Inset index map, depth map to base of MTC (Fig. 6A)

sliding to the south-southeast. It is possible that this structural style becomes the dominant one in the upper part of the translational domain.

Correlation of hanging-wall and footwall cutoffs across the two major frontal ramps in the compressional domain indicates a combined lateral displacement (shortening) of 6.3 km (Figs. 7, 16, and 17). However, the effects of structural compaction in deep-water fold and thrust belts can contribute as much as 40% shortening (Moore et al., 2011), so the correlation method may be a significant underestimate. Another way to estimate shortening is by using the depth to detachment method (e.g., Epard and Groshong, 1993). In Figure 7B an area of the MTC of 8.7 km has been uplifted above a regional line. If the maximum depth to detachment is used (1.7 km), then the amount of shortening estimated is 5.1 km; if an average depth to detachment (1.3 km) is applied, then the amount of estimated shortening is 6.7 km. These shortening values are underestimates because the area above the regional line has probably been reduced post-MTC emplacement by scouring, vertical compaction, and extensional collapse. However, the estimates lend support to the calculation of ~6–7 km of shortening, based on offsets at the frontal ramps. The ability to correlate the stratigraphy across the western lateral ramp with only minor stratigraphic separation also suggests that the large coherent slide blocks did not move very far laterally (i.e., kilometers, not tens of kilometers).

The general north-northwest to south-southeast transport direction of the MTC is defined by the orientations of the lateral and frontal ramps and fold and imbricate structures (Figs. 8 and 24). Locally in the southeast part of the core area at the oblique ramp the transport direction is more to the southeast, indicating radial transport at the compressional region of the MTC. Assuming similar bathymetry at the time of the MTC emplacement to the present, the western lateral apron was emplaced upslope relative to the core area, while the eastern lateral apron was emplaced downslope (Figs. 2 and 3). Therefore, movement against gravity versus movement with gravity appears to explain why the extent of the western and eastern lateral aprons is different.

The geometric patterns and kinematics of the faults can be recognized in each part of the coherent MTC. The lateral continuity or strike of the faults can be traced in detail using mapping from vertical seismic lines, RMS maps, and time slices in the 3D seismic area, which can be used as a model for the other areas covered only by 2D. In this way the overall fault patterns can be generated (Fig. 24). The general fault patterns of the MTC indicate that movement in the upper slope to the middle part of the core area is an extensional regime driven by gravity, which becomes compressional downslope. Fault patterns show a relatively similar style to the fault pattern in the slump internal geometry model by Debacker et al. (2009), with some modifications and added complexities. The additional modifications of the fault patterns in this MTC are normal faults pattern in the flank domain, thrust faults in the lateral apron domain, and antithetic-synthetic normal faults that postdate, and are superimposed on, thrusts. Imbricate thrust system form fold-related pressure ridges in the distal part of the frontal apron domain (Figs. 22 and 23).

Figure 25 is a generalized interpreted model of the stages in development of the MTC. Figure 25B highlights the changes in stress during initial movement of the MTC. As the sliding mass moves downdip, it becomes laterally constrained due to decreasing sliding energy.

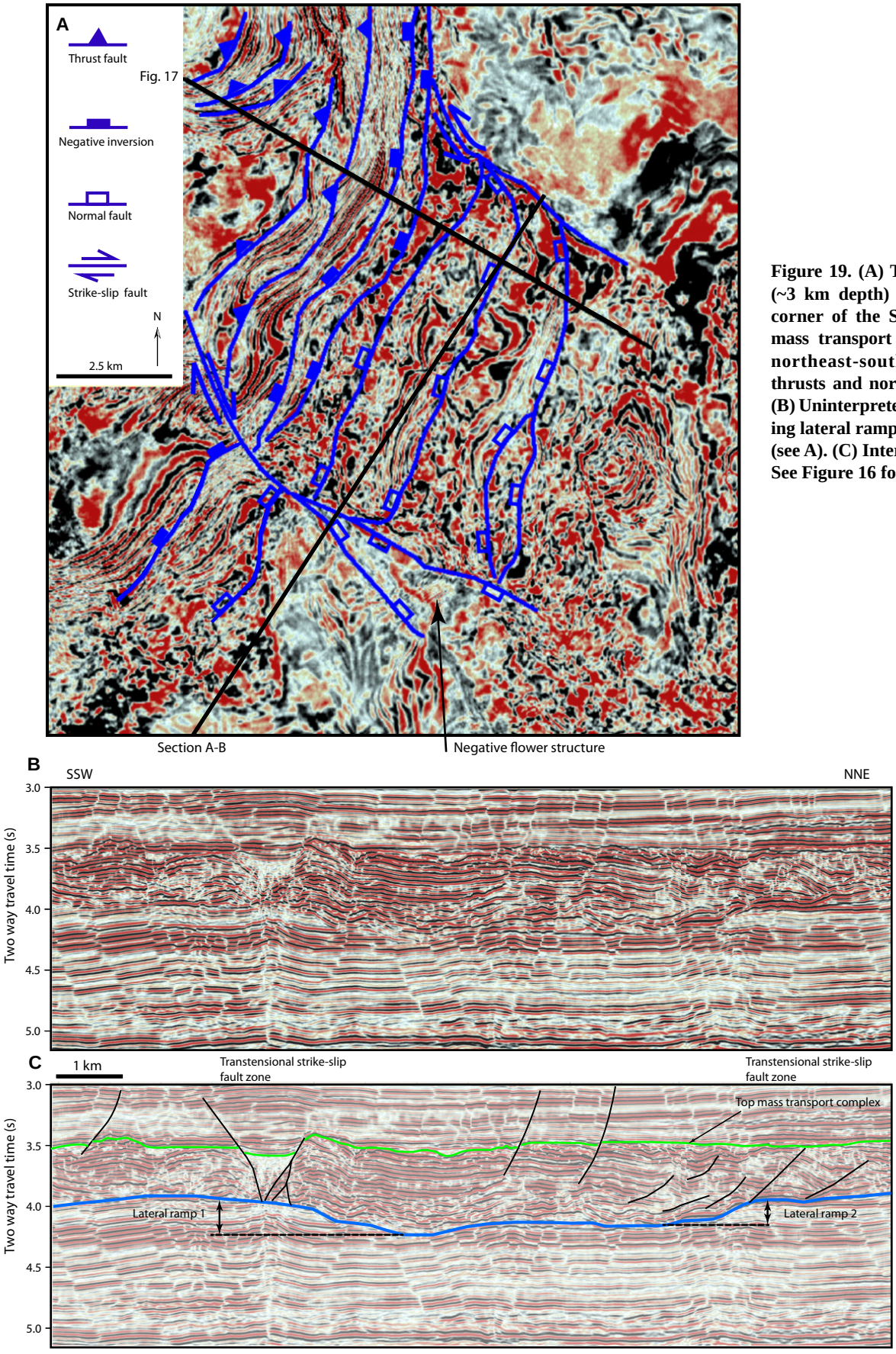

Figure 19. (A) Time-slice map at 4.0 s (~3 km depth) through the southeast corner of the South Makassar Strait mass transport complex, showing the northeast-southwest orientation of thrusts and normal faults in the area. (B) Uninterpreted seismic section showing lateral ramps developed in the area (see A). (C) Interpreted seismic section. See Figure 16 for location.

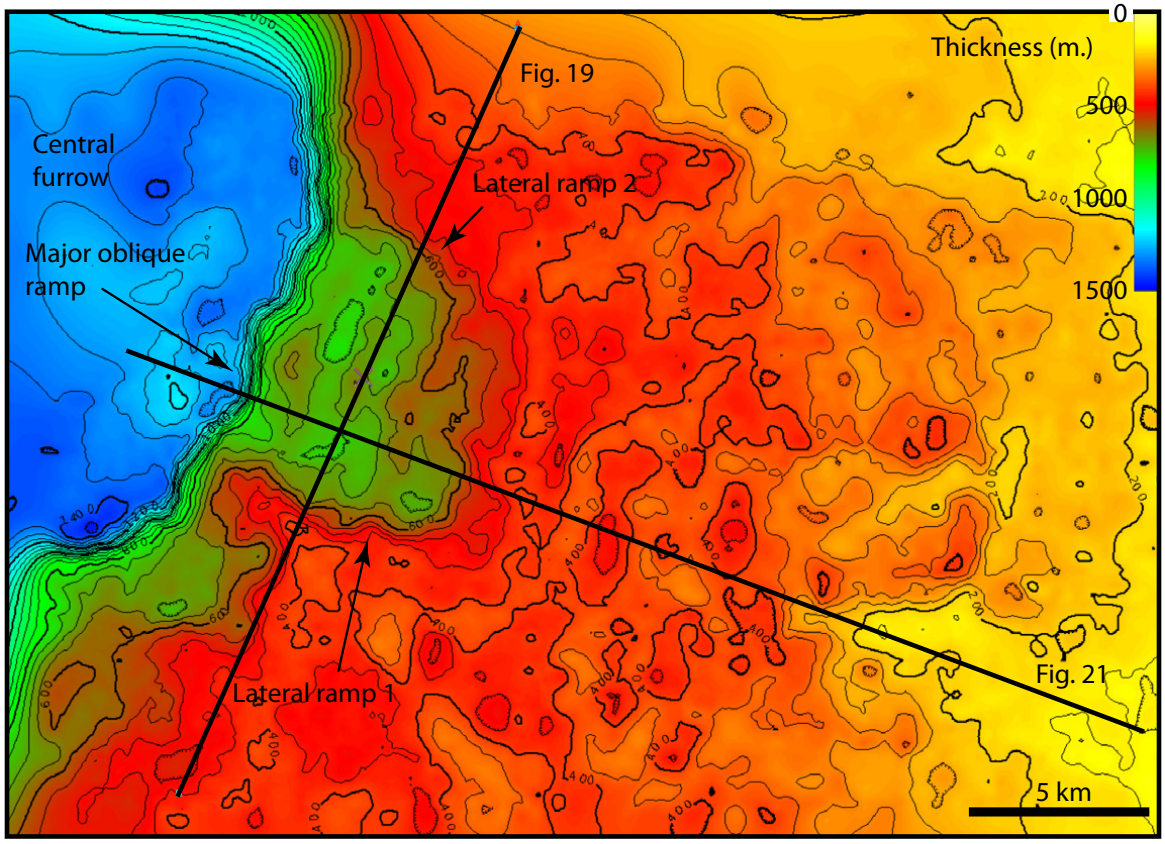

Figure 20. Isopach map of the South Makassar Strait mass transport complex in the southeast area based on mapping of three-dimensional seismic data (see Fig. 8 for location).

A thrust system transported the MTC material up the lateral ramps and a frontal ramp (Fig. 25B). There were two stages of frontal ramp propagation (Figs. 25B, 25C). The second stage resulted in deformation beyond the footwall ramp of a much thinner sedimentary sequence, which forms the frontal apron domain of the MTC. The varied internal structures developed in the frontal apron form three main subdomains (Fig. 8). Much of the frontal apron domain is imbricated (Fig. 22), and becomes progressively thinner away from the lateral and frontal ramps in the toe domain (Fig. 24).

Negative inversion is observed in areas around the frontal ramps in the toe and frontal apron domain, where extensional reactivation of the imbricate thrusts has occurred (cf. Figs. 25B–25D). The stress change is interpreted to be due to energy decrease or cessation of sliding movement from upper slope, so that the overthickened bulge of sediment collapsed under its own weight back toward the core area. This dip of faults toward the center of the MTC suggests that the extensional collapse was triggered by some process within the core area. It is possible that fluid loss and compaction drove the collapse. The post-MTC sedimentary strata show draping over and onlap onto the top MTC (Fig. 25E). These sediments thin onto the thickest and highest morphology parts of the MTC.

DISCUSSION

The South Makassar Strait MTC is a slope-attached type following the scheme of Moscardelli and Wood (2008). The 3D seismic data around the extensional headwall region, and 2D and 3D seismic data in the compressional toe area, show the presence of faulted blocks with coherent internal stratigraphy. The shortening estimates of ~6 km from the toe region (see Interpretation discussion), the coherent internal stratal geometries, and the slope-attached nature of the MTC all indicate that it is a slide, predominantly composed of coherent internal stratigraphy that has undergone relatively low internal translation (kilometers, not tens of kilometers). There are places in the 3D seismic data in the headwall area where amplitudes dim, and it becomes more difficult to detect the internal stratigraphy. Whether this reflects that the sediments have laterally become less coherent (i.e., more like a slump or debris flow) or they are less well imaged in seismic data, but in reality are still predominantly coherent (perhaps due to increasing fault density, higher degree of bed rotation, gas effects), is uncertain. However, the presence of discontinuous high-amplitude events hundreds of meters long, showing varying degrees of rotation, suggests that much of the extensional and translational area is composed of complex faulted, coherent rotated blocks, rather than a rock volume whose internal stratigraphy has been completely lost. The resolution of 2D data is lower than that of the 3D data, and so it is not considered a reliable indicator of the internal continuity of beds within the MTC in areas of low, or apparently chaotic reflections. It is notable that in Figure 14 the internal stratigraphy of the faulted blocks is clearly visible except for the easternmost area block, which loses much of its internal reflectivity. In other parts of the same section there is a lateral transition from high- to low-amplitude (light colored; Fig. 14) units that still preserve internal reflector continuity. The loss of reflectivity can be related to the effects of shallow gas, marked irregularities at the top of the MTC,

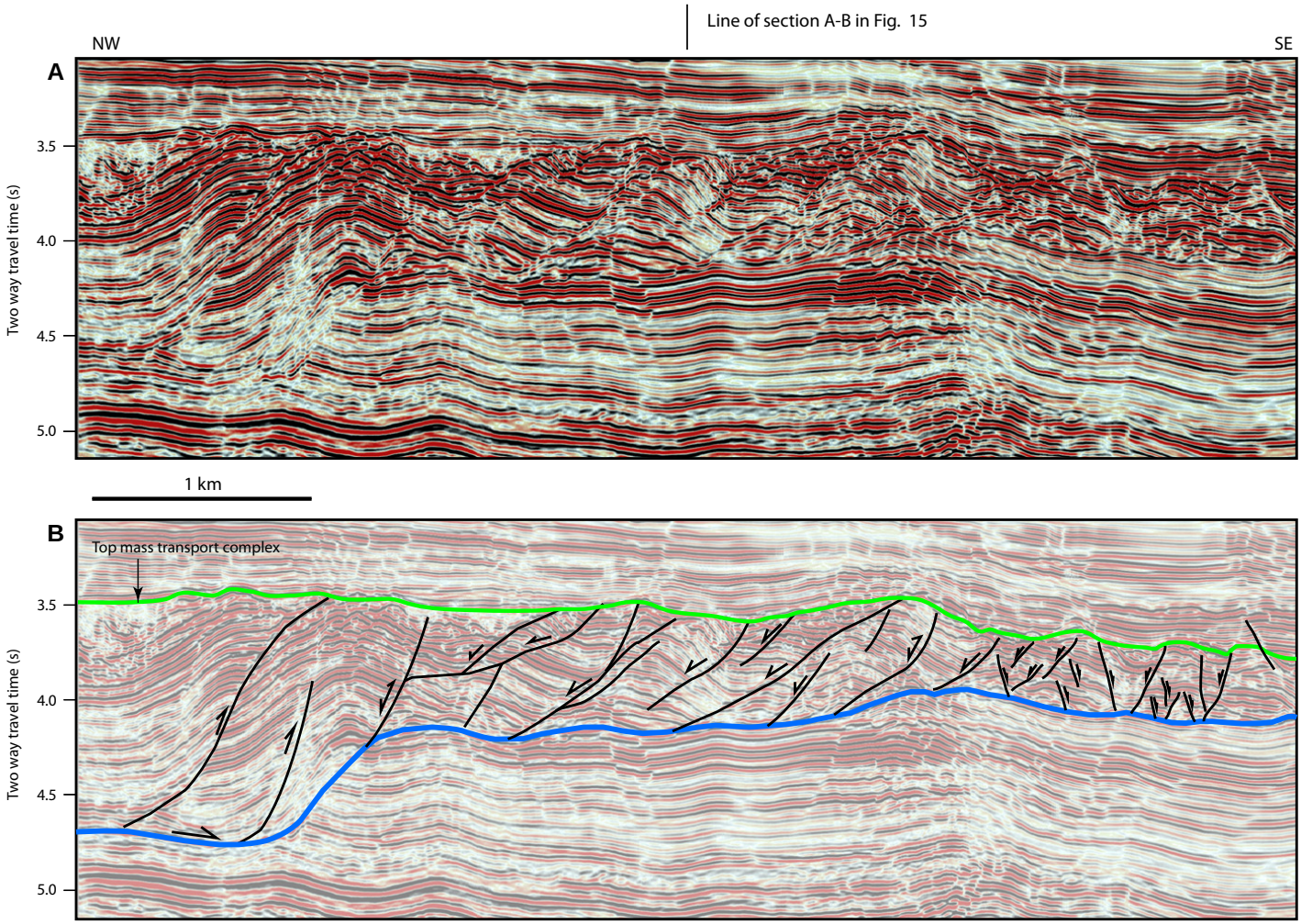

Figure 21. (A) Uninterpreted northwest-southeast arbitrary line through three-dimensional seismic survey 2 (Fig. 6), showing the oblique ramp area on the eastern margin of the core area. (B) Interpreted line. The imbricate thrusts are present west of the main basal thrust ramp. Later extensional collapse has affected the southeast part of the line. The normal faults pass from primarily dipping to the northwest to mixed northwest and southeast dips to the southeast. See Figure 16 for location.

intense faulting, and high dips within the MTC. It is therefore possible to argue that slightly more complex deformation in one fault block would cause it to appear chaotic compared with its neighbors (particularly in 2D data).

It is argued here that the South Makassar Strait MTC was predominantly emplaced as a slide, which implies a weak basal detachment. The large relatively undeformed blocks along the edges of translational and toe domains have similar dips at their top and base (±0.40°), thus there is no critical-taper wedge development (Xiao et al., 1991). However, in the headwall and translational domain, low-taper (2°–3°) wedge geometries are observed. The relatively gentle basal dip of the MTC in the headwall to translational domain (~2°–4°) indicates a very small basal friction angle, which corresponds to a very small coefficient of sliding friction, caused by either clayey gouge (Davis and Reynolds, 1996) or by high pore fluid pressure. The sedimentary strata of the MTC are weak, and poorly lithified, and the presence of extensive polygonal faults in the basin (Fig. 26) suggests the potential for fluid expulsion events below the MTC that could have caused high pore fluid pressures. The possibility of overpressure causing instability on the MTC basal detachment plane is also indicated by fluid escape features in the sedimentary strata below the MTC (Fig. 9B). A high-pressure zone was encountered in the MTC interval in Well X, where 14–16 ppg drilling mud was used. These data further suggest that overpressured fluids probably played a role in the MTC deformation, although the modern overpressure may also be a later phenomenon. A subtle change in lithology may also have helped guide the location of the basal detachment. In Figure 5 it can be seen that unit 1 consists of more limestone stringers than unit 2. Because the limestone stringers were probably lithified earlier than the siltstone stringers of unit 2, the basal detachment location may have been influenced by a change in relative strength of the two units.

Frey-Martinez et al. (2006) discussed the development of compression structures in the toe regions of sliding masses, and noted arguments for different sequencing of deformation within the toe. Thrusts may propagate from the front to the rear of the translating mass (backstepping; Farrell, 1984), or frontward and outward with time (Martel, 2004). The propagation of an imbricate thrust from the lower thrust (Fig. 16; thrust 2), to cut the higher, more internal thrust (Fig. 16; thrust 1) indicates that for the South Makassar Strait MTC the sequence

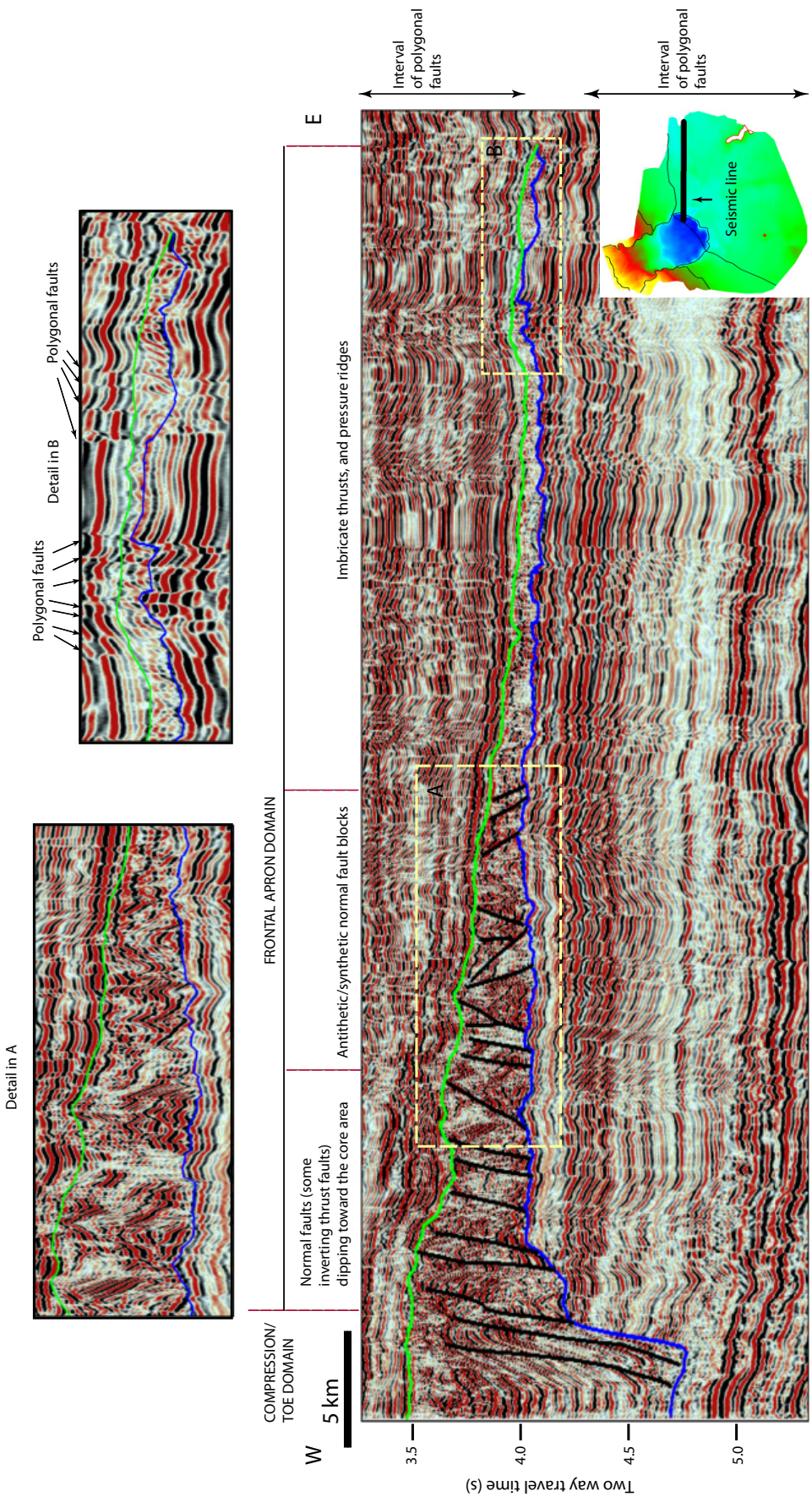

Figure 22. East-west three-dimensional seismic line through the outer wedge showing the change in style from the inner to the outer part of the eastern apron area. Inset index map, depth map to base of MTC (Fig. 6A).

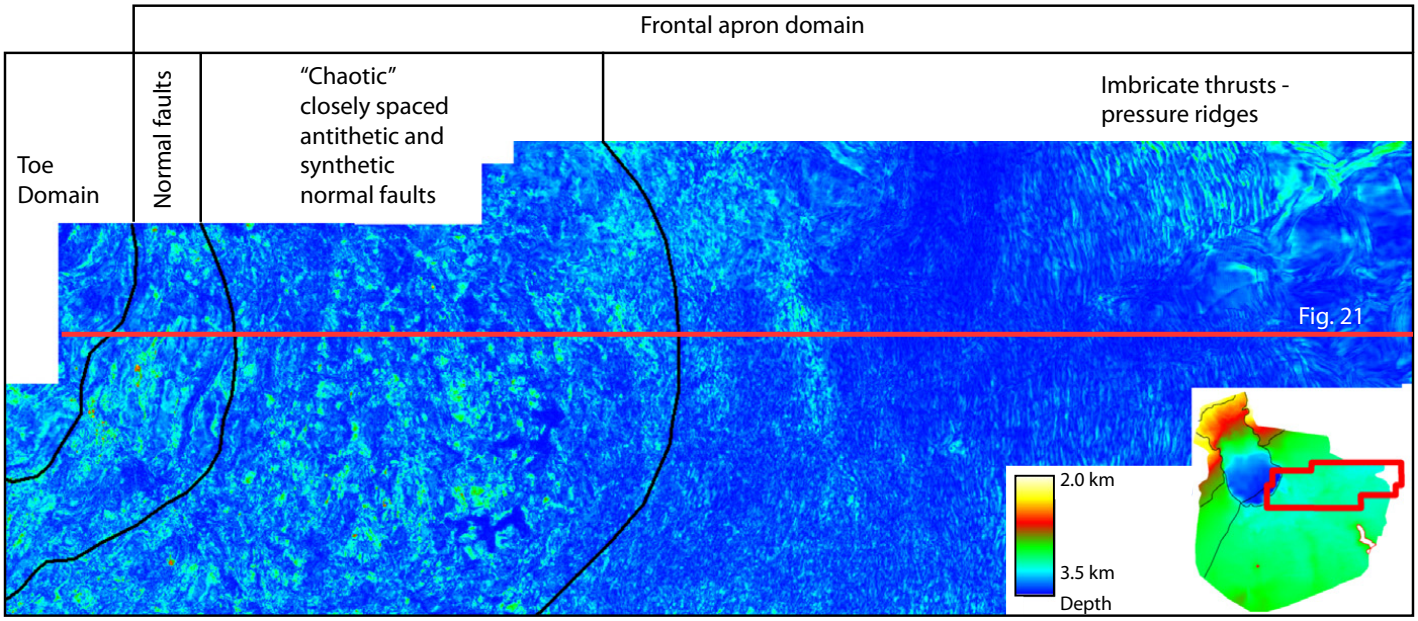

Figure 23. Root mean square (RMS) amplitude time-slice map through the mass transport complex showing the lateral variation in reflection character in the apron area, from poorly organized reflectivity in the west to short wavelength, but regular reflections in the area of imbricate thrusts and pressure ridges. Inset index map, depth map to base of MTC (Fig. 6A).

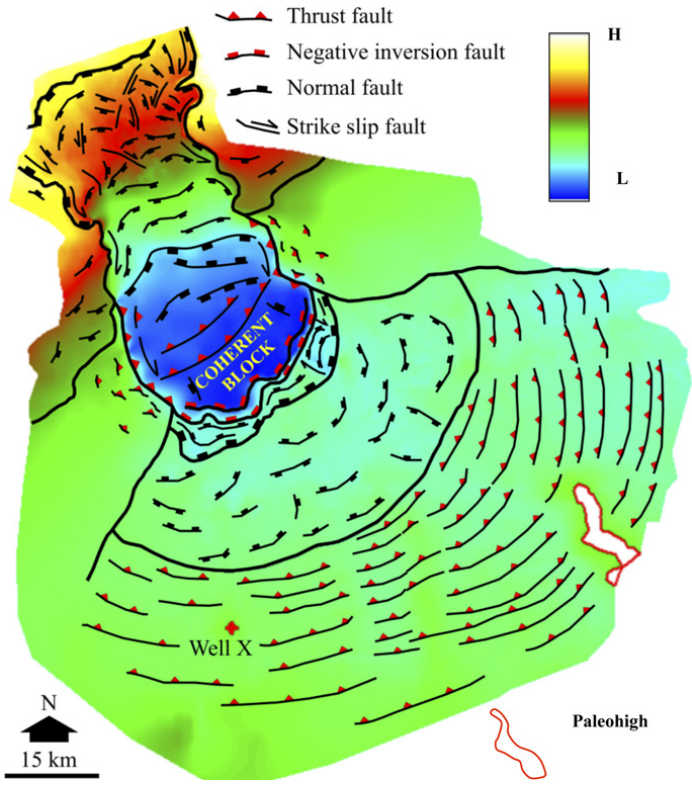

Figure 24. Map of schematic structural zones superimposed on time-structure map of the base mass transport complex. H—high; L—low.

of deformation was outward (i.e., basinward) with time.

Frey-Martinez et al. (2006) discussed that some landslides terminate downdip without ramping up (frontally confined), whereas others ramp up, and exhibit considerable surface relief around the ramp (frontally emergent). Frey-Martinez et al. (2006) also noted that frontally emergent submarine landslides may travel freely over the undeformed slope position, possibly evolving into debris flows and turbidity currents. Frontally confined submarine landslides also tend to preserve internal stratification (e.g., subhorizontal reflections and blocks of intact strata). In the end-member cases described by Frey-Martinez et al. (2006), the frontally emergent landslide is accompanied by evacuation of the headscarp area, whereas the headscarp is not evacuated in the frontally confined case. The South Makassar Strait MTC is a hybrid case, but is closer to the frontally confined end member than the frontally emergent one.

The contractional region of the South Makassar Strait MTC is composed almost entirely of coherent stratigraphy that in places has been imbricated, and in other places thrust as a large sheet (Figs. 16 and 17). Even the apron area with its thin section appears to be mostly composed of imbricate thrusts (Fig. 22B), but this region is just at or below the resolution of the seismic data, so the picture is not absolutely clear.

Well to seismic correlation indicates that the interval velocity of sedimentary unit 1 (Fig. 5) is

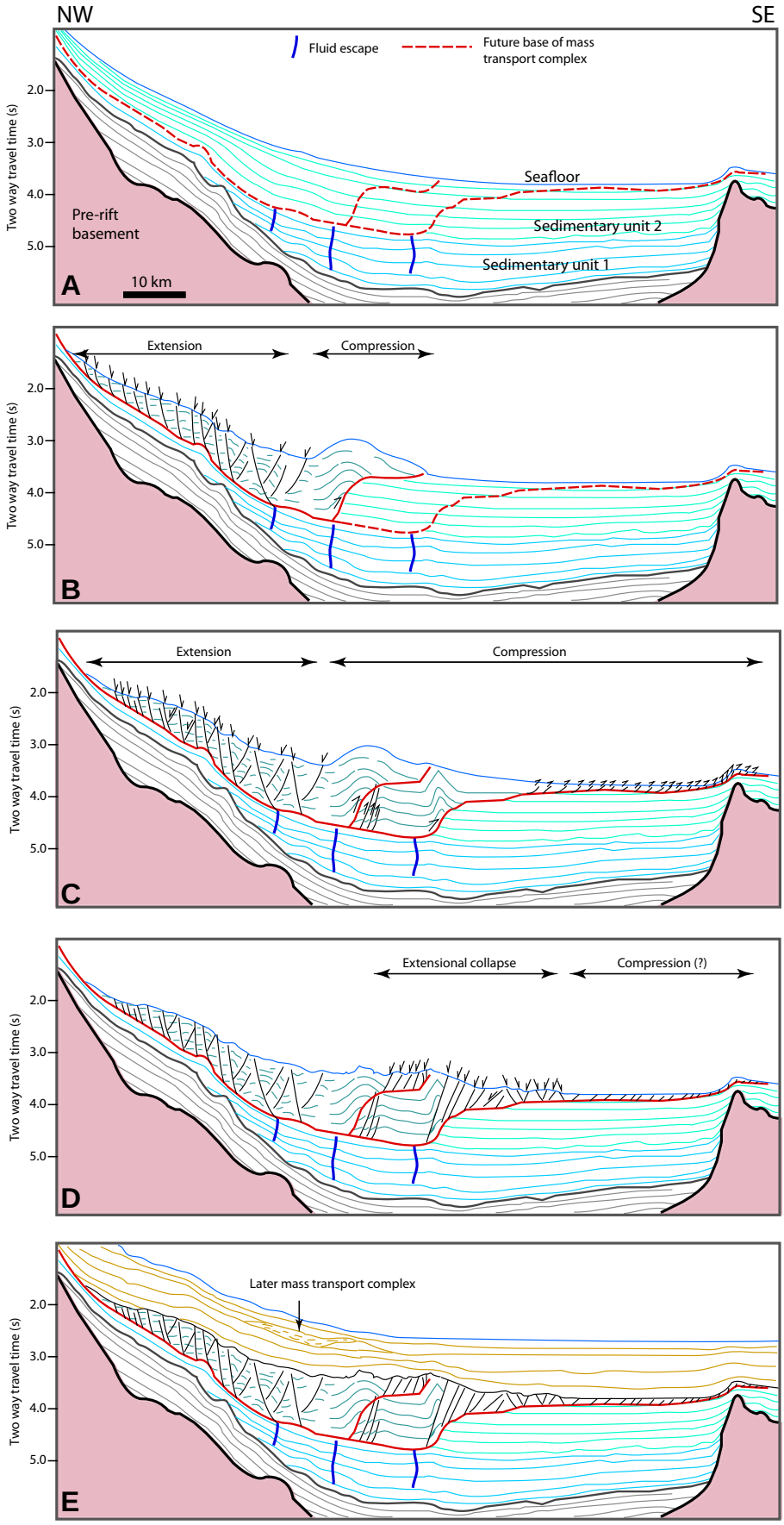

Figure 25. Stages of development of the South Makassar Strait mass transport complex (MTC). (A) Initial stage prior to movement. (B) Sliding and creation of extensional and compressional regions of the MTC during the early Pliocene. (C) Further sliding, and creation farther downslope of a second ramp, and extensive imbrication in the apron area. (D) Extensional collapse of the outer part of the compressional belt, which probably fed into renewed or new compression in the outermost toe area. (E) Burial of the MTC by subsequent sedimentation during the Pliocene–Holocene.

slow (2045 m/s), which requires the sediments to have a high water content and high porosity even after burial and deformation. Therefore at the time of deformation the sediments, like the present-day overburden, must have been very water rich and weak. Conversely, the coherent internal structures indicate that large sedimentary blocks were translated without disintegrating. The presence of a wedge-shaped morphology in parts of the MTC also indicates that the wedge has some coherent strength, and would have thickened by internal deformation until critical taper was reached, then lateral sliding could commence. The absence of growth strata associated with growing folds, or with extensional faults at the updip part of the MTC, plus the absence of a clear sedimentary depocenter or indications of a rapidly prograding sedimentary system indicate that the MTC cannot be interpreted as a slowly developing deltaic-type gravity system. However, in places the headscarp region shows evidence that the western part of the extension region was sealed by undeformed sediment relatively early, while normal faults from the MTC cut and deform the undeformed capping sediment in the eastern part of the headscarp area (Fig. 14). Consequently, the slide has slipped over a time period that spans as much as 500 ms TWTT of sediment thickness (~500 m), although probably the bulk of the displacement of the slide occurred during a fraction of this. With reference to Figure 14, the early stage of the slide is interpreted to be a minor creep event before formation of horizon 2 and during formation of unit A. The main slide displacement is interpreted to have occurred during formation of unit B, when locally as much as ~200 m of bedded sediment was deposited, implying that some significant period of time was required for deposition, and sliding was relatively slow. A period of minor reactivation and creep occurred locally during deposition of unit C. The wedge geometry and internal coherent

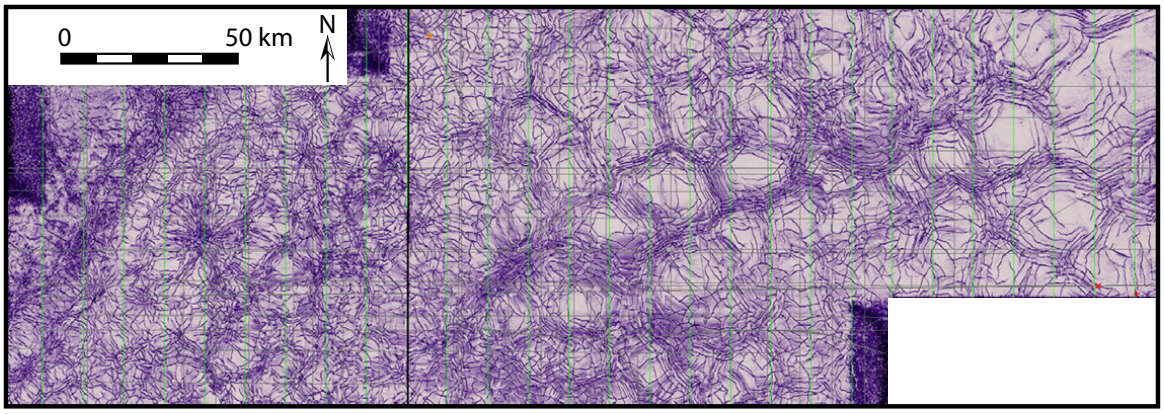

Figure 26. Root mean square (RMS) amplitude time slice showing that the minor faults affecting the section above and below the mass transport complex have a polygonal map-view geometry.

deformation also suggest that the slide is associated with relatively slow strain rates (i.e., it is unlikely the slide developed catastrophically in minutes or hours, but more likely developed by creep over years). Based on the two main thrusts (Figs. 7 and 17), the shortening amount of the MTC is estimated to be a minimum of 6.3 km. Possible analogues for slow strain rate, gravity-driven folds and thrusts in young, weak sedimentary sections, are the Hawaii coherent submarine volcaniclastic MTCs that develop with strain rates between 6 and 60 cm/yr (Morgan et al., 2003). Therefore, the emplacement time for the South Makassar Strait MTC was possibly 10,000 yr. Deposition on this time scale also seems reasonable for the wedge-shaped unit B (Fig. 14B).

One explanation for the hybrid nature of the South Makassar Strait MTC is that it is an amalgamation of more than one slide event. There are small MTCs that within the stratigraphy that are affected by the South Makassar Strait MTC (Figs. 10 and 11). However, these MTCs are too small and geographically limited to be responsible for the apron area; they are interpreted to represent part of the prekinematic stratigraphy. Although in some areas of the toe region it looks as if an upper chaotic unit can be separated from the underlying units, detailed mapping of such boundaries shows no consistent, separate upper MTC unit that can be mapped around. The apron area grades laterally gradually into the thicker sequences of the core area, and cannot be separated by any clear boundary. It therefore appears to have been emplaced as one mass, albeit relatively slowly, and in a number of stages.

A comparison of the South Makassar Strait MTC to others based on its size, internal characteristics, and the emplacement processes is provided in Table 1. The volume of the South Makassar Strait MTC is 2438 km^3 and it covers a total area of ~8985 km^2. With reference to Gee et al. (2007), who compared the largest MTCs identified worldwide, the South Makassar Strait MTC would rank as the second largest in terms of volume and the third largest in terms of areal extent. Since 2007 two areas of mega-MTCs have been described. Silva et al. (2010) reported two megaslides on the Amazon Fan, each covering >80,000 km^2 (Fig. 27). Northeast of the Storegga slide along the Barents Sea margin, Hjelstuen et al. (2007) described three Pleistocene megafailures, the two largest of which each cover an area of ~120,000 km^2 and involve 25,000 km^3 of sediment. Both Silva et al. (2010) and Hjelstuen et al. (2007) showed evidence for closely spaced imbricate thrusts within parts of the MTC complexes. The giant chaotic body offshore northwest Morocco, the offshore extension of the onshore pre-Rifaine nappe (e.g., Torelli et al., 1997), cannot be included in this review because it is not a single body, and has a complex and composite history of development related to thrusting within the Rif-Betic Cordillera (e.g., Morley et al., 2011), as well as being related to a series of MTCs (Iribarren et al., 2007). The measure of area over volume [$A/V^{(2/3)}$] is a measure of the relative efficiency of runout associated with an MTC: the lower the number, the more inefficient the slide (Dade and Huppert, 1998). The Makassar slide is relatively inefficient (Table 1), which is to be expected given the low displacement of the entire complex.

The South Makassar Strait MTC shows predominantly coherent sedimentary strata within the extensional headwall area and the compressional toe region; the nature of the translational area is more debatable. Unfortunately, only relatively low resolution 2D seismic reflection data are available. The internal geometry appears more chaotic, but this may be an issue of seismic resolution in a highly deformed (but still coherent) section. Possibly structural style 7 in the headwall area (Figs. 10A and 13) is analogous for much of the poorly imaged translational area. The extent of the coherent stratigraphy makes the South Makassar Strait MTC unusual when compared to other large MTCs, which mostly consist of debris flows inside the MTC, although imbricates in coherent section are described in places from the toe region, and coherent extensional systems exist in parts of the headwall (Gee et al., 2007; Canals et al., 2004; Frey-Martinez et al., 2005; Silva et al., 2010). Examples of large, purely rotational slides or slumps that show extensive preservation of the original internal structure of the MTC were described by Macdonald et al. (1993), Lee et al. (2004), and Frey-Martinez et al. (2005, 2006). The coherent characteristics of the South Makassar Strait MTC are interpreted to be mainly due to a relatively slow strain rate during emplacement.

CONCLUSIONS

Most mega MTCs are found on high-sedimentation-rate deltaic margins, or passive margins (Brunei slide, Baram Delta—Gee et al., 2007; Para-Maranhao megaslide, Amazon basin—Silva et al., 2010; Barents Sea—Hjelstuen et al., 2007), and were probably rapidly emplaced as debris flows and are associated with many other large debris flows. The South Makassar Strait formed on a relatively slow-sedimentation-rate margin, and is the only MTC complex of its kind on the margin. The setting is a failed rift with sag basin, enhanced by late flexural loading. The trigger was probably gradual uplift of the Paternoster platform, which increased the dip of the headwall region by 2° over the period of slide activity. The result was that a large vol-

TABLE 1. SUMMARY OF THE CHARACTERISTICS OF SOME HUGE MASS TRANSPORT COMPLEXES

Mass transport complex, reference	Geological setting	Volume (km^3)	Area (km^2)	Area/ volume (2/3)	Mass transport complex type	Speculated trigger mechanism
Fos dos Amazonas megaslides (Silva et al., 2010)	Passive (transform) margin	60,000	90,000	59	Debris flow with coherent normal fault blocks and imbricates updip and downdip	Narrow margin, high sedimentation rates from Amazon and other rivers, eustasy, canyon head erosion
Bjornoya fan slide complex (Hjelstuen et al., 2007)	Passive margin	25,000	120,000	140	Mostly debris flow, some imbricated toe areas	Earthquake activity associated with postglacial isostatic rebound; presence of gas and gas hydrates
Storegga (Canals et al., 2004; Bryn et al., 2005)	Passive margin	3000	35,000	169	Mostly debris flow	Earthquake activity associated with postglacial isostatic rebound; presence of gas and gas hydrates
Nuuanu-Wailau debris field (Satake et al., 2002)	Hotspot seamount chain	3000	12,000	58	Debris flow and huge slide blocks	Volcanic activity, earthquakes
South Makassar Strait Basin (this study)	Postrift sag basin, with additional flexural loading from margins	2438	8985	50	Mostly coherent slide; thrust sheets and imbricates	Slow rotation of slope area by ~2°, possibly aided by overpressure from vertically transported fluids
Brunei mass transport complex (Gee et al., 2007)	Delta on inverted postcollisional margin	1200	5300	47	Debris flow	Sediment loading from Baram River and canyon; sediment column weakened by upward-moving fluids; possible anticline collapse; earthquake activity likely
Sahara slide (Georgiopoulou et al., 2010)	Active convergent margin	600	30,000	422	Mostly debris flows; very long runout (~900 km)	Differential compaction and sedimentation across scarps leading to pore pressure instability
BIG'95 (Canals et al., 2004)	Passive margin	26	2000	228	Debris flow	Earthquakes, rapid sedimentation, vertically transported fluids

ume of sediment crept downslope. The major coherent, internal, largely undeformed sections involved in the frontal thrusts indicate that the weak, water-rich, low-velocity (~2000 m/s) sediments were able to slide without breaking down into small blocks, deforming in a ductile fashion or collapsing into debris flows or turbidites. This suggests that movement was slow, and did not occur in minutes or hours, unlike many MTCs. The amount of downslope displacement is not large compared with the tens of kilometers covered by the movement of large, rapidly emplaced, and potentially tsunamigenic MTCs. The offset of horizons at the hanging-wall and footwall cutoffs along two major frontal ramps suggests ~6.3 km displacement. By analogy with Hawaiian submarine slides, a time scale for emplacement of 1000–10,000 yr (~6 cm/yr to 60 cm/yr) is proposed.

The South Makassar Strait MTC has a volume of 2438 km^3; it is possibly the largest

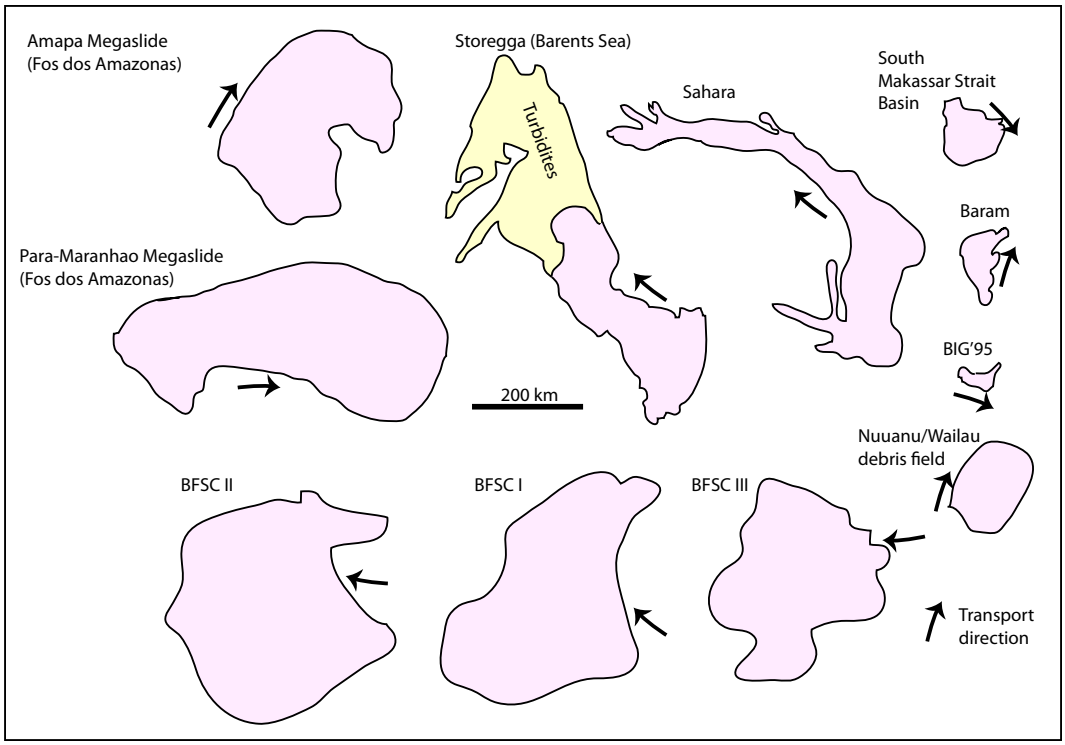

Figure 27. Comparison of the areas of very large mass transport complexes (information from Shipboard Scientific Party, 2003; Gee et al., 2007; Hjelstuen et al., 2007; Silva et al., 2010). BFSC—megaslides of the Bjornoya fan slide complex, Barents Sea (Hjelstuen et al., 2007).

coherent MTC so far described. The morphology is similar to that of other MTCs, exhibiting an extensional headwall area, lateral, oblique, and frontal ramps, a translational domain, and compressional toe. More unusual aspects include the broad imbricated apron domain, and the well-developed extensional faults superimposed on the compressional toe region. The toe region built up as compressional wedge, and then collapsed under extension.

The South Makassar Strait MTC can be classified using existing schemes as a slope-attached (Moscardelli and Wood, 2008) hybrid, but predominantly frontally confined (Frey-Martinez et al., 2006) slide (e.g., Nardin et al., 1979). The trigger mechanism for the slide (regional uplift and rotation) is not among those considered for slope-attached systems by Moscardelli and Wood (2008). The South Makassar Strait MTC can be described as slowly creeping coherent slide, and emphasizes that the time taken to emplace an MTC can also be an important factor in its morphology and development.

ACKNOWLEDGMENTS

Armandita is grateful to the Special Task Force for Upstream Oil and Gas Business Activities Republic of Indonesia (SKKMigas) and PTTEP (PTT Exploration and Production Public Company Limited) for sponsoring this study, Talisman Energy and PTTEP for providing valuable data, and the Directorate General of Oil and Gas–Ministry of Energy and Mineral Resources, Republic of Indonesia, for their permission to utilize the data. We thank L. Moscardelli and an anonymous reviewer for constructive and useful reviews of an earlier version of this manuscript, and Mads Huuse and Joe Cartwright for helpful and constructive reviews.

REFERENCES CITED

Alves, T.M., 2010, 3D Seismic examples of differential compaction in mass-transport deposits and their effect on post-failure strata: Marine Geology, v. 271, p. 212–224, doi:10.1016/j.margeo.2010.02.014.

Armandita, C., Pudyo, N., Saputra, S.E., Sumaryana, and Mukti, M.M., 2011, Exploration challenges and opportunities in deep water Makassar Strait basins, Indonesia: Review of carbonate play based on sequence stratigraphic and seismic characterization: San Antonio, Texas, 2011 Society of Exploration Geophysicists Annual Meeting, 5 p.

Bachtiar, A., Purnama, Y.S., Suandhi, P.A., Krisyunianto, A., Rozalli, M., Nugroho, D.H.H., and Suleiman, A., 2013, The Tertiary palaeogeography of the Kutai Basin and its unexplored hydrocarbon plays: Indonesian Petroleum Association Proceedings, 37th Annual Convention and Exhibition, IPA13-G-126, 37 p.

Bull, S., Cartwright, J., and Huuse, M., 2009, A review of kinematic indicators from mass-transport complexes using 3D seismic data: Marine and Petroleum Geology, v. 26, p. 1132–1151, doi:10.1016/j.marpetgeo.2008.09.011.

Calvert, S.J., and Hall, R., 2003, The Cenozoic geology of the Larian and Karama regions, western Sulawesi: New insight into the evolution of the Makassar Straits region: Indonesian Petroleum Association Proceedings, 29th Annual Convention and Exhibition, IPA03-G-036, 13 p.

Canals, M., Casamor, J.L., Urgeles, R., Lastras, G., Calafat, A.M., Masson, D., Berne, S., Alonso, B., and DeBatist, M., 2000, The Ebro continental margin, Western Mediterranean Sea: Interplay between canyon-channel systems and mass wasting processes, *in* Weimer, P., et al., eds., Deep-water reservoirs of the world: 20th Annual GCS-SEPM Bob F. Perkins Research Conference Proceedings, p. 152–174, doi:10.5724/gcs.00.15.0152.

Canals, M., and 16 others, 2004, Slope failure dynamics and impacts from seafloor and shallow sub-seafloor geophysical data: Case studies from the COSTA project: Marine Geology, v. 213, p. 9–72, doi:10.1016/j.margeo.2004.10.001.

Cloke, I.R., Moss, S.J., and Craig, J., 1997, The influence of basement reactivation on the extensional and inversional history of the Kutai Basin, eastern Kalimantan: Geological Society of London Journal, v. 154, p. 157–161, doi:10.1144/gsjgs.154.1.0157.

Cloke, I.R., Milson, J., and Blundell, D.J.B., 1999, Implications of gravity data from East Kalimantan and the Makassar Straits: A solution to the origin of the Makassar Straits?: Journal of Asian Earth Sciences, v. 17, p. 61–78, doi:10.1016/S0743-9547(98)00056-7.

Dade, W.B., and Huppert, H.E., 1998, Long-runout rockfalls: Geology, v. 26, p. 803–806, doi:10.1130/0091-7613(1998)026<0803:LRR>2.3.CO;2.

Davis, G.H., and Reynolds, S.J., 1996, Structural geology of rocks and region (second edition): New York, John Wiley and Sons, Inc., 776 p.

Debacker, T.N., Dumon, M., and Matthys, A., 2009, Interpreting fold and fault geometries from within lateral to oblique parts of slumps: A case study from Ango-Brabant deformation belt (Belgium): Journal of Structural Geology, v. 31, p. 1525–1539, doi:10.1016/j.jsg.2009.09.002.

Dott, R.H., Jr., 1963, Dynamics of subaqueous gravity depositional processes: American Association of Petroleum Geologists Bulletin, v. 47, p. 104–128.

Dykstra, M., Garyfalou, K., Kertznus, V., Kneller, B., Milana, J.P., Molinaro, M., Szuman, M., and Thompson, P., 2011, Mass-transport deposits: Combining outcrop studies and seismic forward modeling to understand lithofacies distributions, deformation, and their seismic stratigraphic expression, *in* Shipp, R.C., et al., eds., Mass transport deposits in deepwater settings: SEPM (Society for Sedimentary Geology) Special Publication 96, p. 293–310.

Epard, J.L., and Groshong, R.H., 1993, Excess area and depth to detachment: American Association of Petroleum Geologists Bulletin, v. 77, p. 1291–1302.

Farrell, S.G., 1984, A dislocation model applied to slump structures, Ainsa Basin, South Central Pyrenees: Journal of Structural Geology, v. 6, p. 727–736.

Frey-Martinez, J., Cartwright, J., and Hall, B., 2005, 3D seismic interpretation of slump complexes: Examples from the continental margin of Israel: Basin Research, v. 17, p. 83–108, doi:10.1111/j.1365-2117.2005.00255.x.

Frey-Martinez, J., Cartwright, J., and James, D., 2006, Frontally confined versus frontally emergent submarine landslides: A 3D seismic characterization: Marine and Petroleum Geology, v. 23, p. 585–604, doi:10.1016/j.marpetgeo.2006.04.002.

Gee, M.J.R., Uy, H.S., Warren, J.K., Morley, C.K., and Lambiase, J.J., 2007, The Brunei slide: A giant submarine landslide on the North West Borneo margin revealed by 3D seismic data: Marine Geology, v. 246, p. 9–23, doi:10.1016/j.margeo.2007.07.009.

Georgiopoulou, A., Masson, D.G., Wynn, R.B., and Krastel, S., 2010, Sahara Slide: Age, initiation and processes of a giant submarine slide: Geochemistry, Geophysics, Geosystems, v. 11, Q07014, doi:10.1029/2010GC003066.

Hjelstuen, B.O., Eldholm, O., and Faleide, J.I., 2007, Recurrent Pleistocene mega-failures on the SW Barents Sea margin: Earth and Planetary Science Letters, v. 258, p. 605–618, doi:10.1016/j.epsl.2007.04.025.

Ireland, M.T., Davies, R.J., Goulty, N.R., and Moy, D.J., 2011, Thick slides dominated by regular-wavelength folds and thrusts in biosiliceous sediments on the Vema Dome offshore of Norway: Marine Geology, v. 289, p. 34–45, doi:10.1016/j.margeo.2011.08.001.

Iribarren, L., Verges, J., Camurri, F., Fullea, J., and Fernandez, M., 2007, The structure of the Atlantic-Mediterranean transitional zone from the Alboran Sea to the Horseshoe Abyssal Plain (Iberia-Africa plate boundary): Marine Geology, v. 243, p. 97–119, doi:10.1016/j.margeo.2007.05.011.

Kupecz, J., Sayers, I., Tognini, P., Hilman, A., Tanos, C., and Ariyono, D., 2013, New insights into the tectono-stratigraphic evolution of the South Makassar Basin: Indonesian Petroleum Association Proceedings, 37th Annual Convention and Exhibition, IPA13-G-158, 30 p.

Lastras, G., DeBlasio, F.V., Canals, M., and Elverhoi, A., 2005, Conceptual and numerical modeling of the BIG'95 debris flow, Western Mediterranean Sea: Journal of Sedimentary Research, v. 75, p. 784–797, doi:10.2110/jsr.2005.063.

Lee, C., Nott, J., Keller, F., and Parrish, A., 2004, Seismic expression of the Cenozoic mass transport complexes, deepwater Tarfaya-Agadir Basin, offshore Morocco: Annual Offshore Technology Conference Proceedings, 16741, doi:10.4043/16741-MS.

Macdonald, D., Moncrieff, A., and Butterworth, P., 1993, Giant slide deposits from a Mesozoic fore-arc basin, Alexander Island, Antarctica: Geology, v. 21, p. 1047–1050, doi:10.1130/0091-7613(1993)021<1047:GSDFAM>2.3.CO;2.

Martel, S.I., 2004, Mechanics of landslide initiation as a shear fracture phenomenon, *in* Tappin, D.R., ed., Submarine slump-generated tsunamis: Marine Geology, v. 203, p. 319–339.

Meckel, L.D., III, 2011, Reservoir characteristics and classification of sand-prone submarine mass-transport deposits, *in* Shipp, R.C., et al., eds., Mass transport deposits in deepwater settings: SEPM (Society for Sedimentary Geology) Special Publication 96, p. 423–452.

Miller, K.G., Kominz, M.A., Browning, J.V., Wright, J.D., Mountain, G.S., Katz, M.E., Sugarman, P.J., Cramer, B.S., Christie-Blick, N., and Pekar, S.F., 2005, The Phanerozoic record of global sea-level change: Science, v. 310, p. 1293–1298.

Moore, G.F., Saffer, D., Studer, M., and Pisani, P.C., 2011, Structural restoration of thrusts at the toe of the Nankai Trough accretionary prism off Shikoku Island, Japan: Implications for dewatering processes: Geochemistry, Geophysics, Geosystems, v. 12, doi:10.1029/2010GC003453.

Morgan, J.K., Moore, G.F., and Clague, D.A., 2003, Slope failure and volcanic spreading along the submarine south flank of Kilauea volcano, Hawaii: Journal of Geophysical Research, v. 108, 2415, doi:10.1029/2003JB002411.

Morley, C.K., King, R., Hillis, R., Tingay, M., and Backe, G., 2011, Deepwater fold and thrust belt classification, tectonics, structure and hydrocarbon prospectivity: A review: Earth-Science Reviews, v. 104, p. 41–91, doi:10.1016/j.earscirev.2010.09.010.

Moscardelli, L., and Wood, L., 2008, New classification system for mass transport complexes in offshore Trinidad: Basin Research, v. 20, p. 73–98, doi:10.1111/j.1365-2117.2007.00340.x.

Mosher, D.C., Moscardelli, L., Shipp, R.C., Chaytor, J.D., Baxter, C.D.P., Lee, H.J., and Urgeles, R., 2010, Submarine mass movements and their consequences, *in* Mosher, D.C., et al., eds., Submarine mass movements and their consequences: Advances in Natural and Technological Hazards Research Volume 28: Dordrecht, Springer, p. 1–8.

Nardin, T.R., Hein, F.J., Gorsline, D.S., and Edwards, B.D., 1979, A review of mass movement processes, sediment and acoustic characteristics, and contrasts in slope and base-of-slope systems versus canyon–fan–basin floor systems, *in* Doyle, L.J., and Pilkey, O.H., eds., Geology of continental slopes: Society of Economic Paleontologists and Mineralogists Special Publication 27, p. 61–73, doi:10.2110/pec.79.27.0061.

Nissen, S.E., Haskell, N.L., Steiner, C.T., and Cotterill, K.L., 1999, Debris flow outrunner blocks, glide tracks and pressure ridges identified on the Nigerian continental slope using 3D seismic coherency: Leading Edge, v. 18, p. 595–599, doi:10.1190/1.1438343.

Petersen, M., Harmsen, S., Mueller, C., Haller, K., Dewey, J., Luco, N., Crone, A., Lidke, D., and Rukstales, K., 2007, Documentation for the Southeast Asia Seismic Hazard Maps: U.S. Geological Survey Administrative Report September 30, 2007, 67 p.

Pireno, G.E., and Darussalam, D.N., 2010, Petroleum system overview of the Sebuku Block and the surrounding area: Potential as a new oil and gas province in South Makassar Basin, Makassar Strait: Indonesian Petroleum Association Proceedings, 34th Annual Convention and Exhibition, IPA10-G-169, 16 p.

Satake, K., Smith, J.R., and Shinozaki, K., 2002, Three-dimensional reconstruction and tsunami model of the Nuuanu and Wailau giant landslides, Hawaii, *in* Takahashi, E., et al., eds., Hawaiian volcanoes: Deep underwater perspectives: American Geophysical Union Geophysical Monograph 128, p. 333–346, doi:10.1029/GM128p0333.

Satyana, A.H., 2010, Crustal structures of the eastern Sundaland's rifts, central Indonesia: Geophysical constraints and petroleum implications: Bali 2010 International Geosciences Conference and Exposition Proceedings, 10 p.

Satyana, A.H., and Armandita, C., 2008, On the origin of the Meratus uplift, southeast Kalimantan—Tectonic and gravity constraints: A model for exhumation of collisional orogen in Indonesia: Indonesian Association of Geophysicists 33rd Annual Convention and Exhibition Proceedings, PIT33-OP-022, p. 260–263.

Shipboard Scientific Party, 2003, Leg 200 Summary, *in* Stephen, R.A., et al., eds., Proceedings of the Ocean Drilling Program, Initial Reports, Volume 200: College Station, Texas, Ocean Drilling Program, p. 1–73, doi:10.2973/odp.proc.ir.200.101.2003.

Shipp, C.R., Nott, J.A., and Newlin, J.A., 2004, Physical characteristics and impact of mass transport complexes on jetted conductors and suction anchor piles: Offshore Technology Conference Paper 16751, 11 p., doi.org/10.4043/16751-MS.

Silva, C.G., Araujo, E., Reis, A.T., Perovano, R., Gorini, C., Vendeville, B.C., and Albuquerque, N., 2010, Megaslides in the Foz do Amazonas Basin, Brazilian Equatorial Margin, *in* Mosher, D.C., ed., Submarine mass movements and their consequences: Advances in Natural and Technological Hazards Research Volume 28: Dordrecht, Springer, p. 581–592.

Tanos, C.A., Kupecz, J., Lestari, S., Warren, J.K., and Baki, A., 2012, Depositional and diagenetic effects on reservoir properties in carbonate debris deposits: Comparison of two debris flow within the Berai Formation, Makassar Strait, Indonesia: American Association of Petroleum Geologists International Convention and Exhibition, Search and Discovery Article 90155, 29 p.

Torelli, L., Sartori, R., and Zitellini, N., 1997, The giant chaotic body in the Atlantic Ocean off Gibraltar: New results from a deep seismic reflection survey: Marine and Petroleum Geology, v. 14, p. 125–138, doi:10.1016/S0264-8172(96)00060-8.

Watts, P., 1998, Wavemaker curves for tsunamis generated by underwater landslides: Journal of Waterway, Port, Coastal, and Ocean Engineering, v. 124, p. 127–137, doi:10.1061/(ASCE)0733-950X(1998)124:3(127).

Watts, P., 2003, Probabilistic analyses of landslide tsunami hazards, *in* Locat, J., and Mienert, J., eds., Submarine mass movements and their consequences: Advances in Natural and Technological Hazards Research Volume 19: Dordrecht, Kluwer, p. 163–170.

Wright, S.G., and Rathje, E.M., 2003, Triggering mechanisms of slope instability and their relationship to earthquakes and tsunamis: Pure and Applied Geophysics, v. 160, p. 1865–1877, doi:10.1007/s00024-003-2410-4.

Xiao, H.B., Dahlen, F.A., and Suppe, J., 1991, Mechanical of extensional wedges: Journal of Geophysical Research, v. 96, no. B6, p. 10,301–10,318, doi:10.1029/91JB00222.

Yamada, Y., Kawamura, K., Ikehara, K., Ogawa, Y., Urgeles, R., Mosher, D., Chaytor, J., and Strasser, M., 2011, Submarine mass movements and their consequences, *in* Yamada, Y., et al., eds., Submarine mass movements and their consequences: Advances in Natural and Technological Hazards Research Volume 31: Dordrecht, Springer, p. 1–12, doi:10.1007/978-94-007-2162-3_1.